A unique No-Go Decay cleavage in mRNA exit-tunnel of ribosome produces 5'-OH ends phosphorylated by Rlg1

Albertas Navickas[1#•], Sébastien Chamois[1#], Rénette Saint-Fort[1], Julien Henri[1], Claire Torchet[1], and Lionel Benard[1]*

[1]Institut de Biologie Physico-Chimique, UMR8226, CNRS, Sorbonne Université, Paris, France

[#]Co-first authors

***Corresponding author:** Lionel BENARD, e-mail address: lionel.benard@ibpc.fr

[•]present address: Department of Biochemistry and Biophysics
University of California, San Francisco
San Francisco, CA 94158, USA

Keywords:

No-Go Decay, mRNA surveillance, Endoribonuclease, 5'-hydroxyl RNA, Rlg1, Trl1, Exoribonuclease, Xrn1, Dxo1, disome, Ribosomal mRNA exit tunnel

ABSTRACT

The No-Go Decay (NGD) mRNA surveillance pathway degrades mRNAs containing stacks of stalled ribosomes. An endoribonuclease has been proposed to initiate cleavages upstream of the stall sequence. However, the production of two RNA fragments resulting from a unique cleavage has never been unambiguously demonstrated. We used mRNAs expressing a 3'-ribozyme to produce truncated transcripts *in vivo* to mimic naturally occurring truncated mRNAs known to trigger NGD and produce more precise ribosome stalling events and cleavages than mRNAs containing contiguous rare codons. This technique allowed us to analyse ribosome associated NGD cleavage products at single-nucleotide resolution. We show that (i) the 5'-3' exoribonuclease Xrn1 is the principal contributor to NGD fragment production and (ii) we can detect endonucleolytic cleavage events starting at the third collided ribosome. This cleavage, which we show to be Hel2-dependent, maps precisely in the mRNA exit tunnel of the ribosome, 8 nucleotides upstream of the first P-site residue. A similar analysis of mRNAs containing rare codons showed that at least 3 stacked ribosomes are also necessary for endonucleolytic cleavage of these mRNAs. However, we observed that NGD RNA fragments can also be trimmed by the 5'-3' exoribonuclease activity of Dxo1, creating new extremities in the region theoretically covered by disomes. Finally, we show that NGD endonucleolytic cleavage produces 5'-hydroxylated RNA fragments requiring 5'-phosphorylation prior to digestion by 5'-3' exoribonucleases. We identify the RNA kinase Rlg1/Trl1 as a new essential player in the degradation of NGD RNAs.

INTRODUCTION

The No-Go Decay (NGD) mRNA surveillance pathway degrades mRNAs containing stalled ribosomes [1,2]. NGD occurs when translation elongation is blocked by the presence of stable intra- or intermolecular RNA structures, enzymatic cleavage, chemically damaged sequences, rare codons or mRNA depurination [1,3-8]. This mRNA degradation process is dependent on translation and involves an endoribonuclease that cleaves just upstream of the stall sequence [1,5,6,9]. Other mRNA surveillance pathways can also ultimately lead to NGD. For instance, transcripts synthesized without a stop codon due to premature polyadenylation have stalled ribosomes that are initially detected by the Non-stop decay (NSD) decay pathway [9,10]. NSD targeted mRNAs are cleaved by an uncharacterized mechanism and become targets of NGD when ribosomes reach the new 3'-end and stall [9,11,12]. NGD thus plays a key role in resolving translational issues potentially detrimental to cellular homeostasis. When mRNAs are truncated, the stalled ribosomes are rescued in a process mediated by the Dom34/Hbs1 complex that dissociates the ribosomal subunits [5]. Their association with the 60S subunit is recognized by the Ribosome Quality Control (RQC) pathway leading to the rapid degradation of the nascent peptide [13-15]. However, despite extensive study, the precise location of NGD cleavage and the mechanism of degradation of the resulting RNA fragment remain elusive.

In this paper, we focused on the fate of NGD-cleaved mRNAs, with an initial goal of mapping the sites of mRNA cleavage with accuracy. Two major obstacles to achieving this objective are that NGD fragments are rapidly attacked by 5'-3' and 3'-5' exoribonucleases after ribosome dissociation [5] and that simultaneously blocking the 5'-3' and 3'-5' exoribonuclease decay pathways is synthetically lethal [16]. It has been shown, however, that the stability of such mRNAs is largely dependent on the Dom34/Hbs1 complex [5,17]. In *dom34* mutant cells, ribosomes stalled at the 3'-end of truncated mRNAs inhibit the degradation by the exosome and facilitate the detection of sequential endonucleolytic cleavages upstream of the ribosomal stall site [5]. Interestingly, *dom34* and *xrn1* mutations (inactivating the main 5'-3' exonucleolytic degradation pathway) are not synthetic lethal [1]. Moreover, NGD endonucleolytic cleavages still occur in the absence of Dom34 [2,3]. The limited 3'-5' degradation of specific mRNA targets (in the absence of Dom34) combined with 5'-3' exoribonuclease mutants thus allows an accumulation of RNA fragments resulting from endonucleolytic cleavages whose extremities can be mapped accurately. We created truncated mRNAs *in vivo* by insertion of a hammerhead ribozyme sequence (Rz), known to generate

NGD targeted mRNAs [5]. This construction mimics chemically or enzymatically cleaved mRNAs, or those resulting from abortively spliced mRNAs that are processed by the NGD pathway [5,9,18]. As anticipated, these designed truncated 3'-ends block ribosomes at determined positions and, because ribosomes guide NGD mRNA cleavages [5,19], we were able to detect 3'-NGD RNA fragments of specific sizes. By analysing these RNAs in detail, we show the importance of the 5'-3' exoribonuclease Xrn1 in the production of 3'-NGD fragments. We can perfectly match a 3'-NGD cleavage product with a 5'-NGD cleavage fragment in the region of the third stalled ribosome. We mapped this site and show that a unique endonucleolytic cleavage occurs 8 nucleotides (nts) upstream of the first P-site nt within the third stacked ribosome. The two leading ribosomes are apparently not competent for this cleavage. We demonstrate that this 3'-NGD RNA has a hydroxylated 5'-extremity and show that 5'-phosphorylation by the Rlg1/trl1 kinase [20] is required to allow degradation by 5'-3' exoribonucleases. Interestingly, in the absence of Xrn1, the alternative 5'-3' exoribonuclease Dxo1 takes over [21]. We also analysed mRNAs containing rare codons and at least three stacked ribosomes are required for endonucleolytic cleavage of these mRNAs. We show that 5' ends observed in regions covered by disomes are the result of 5'-3' exoribonucleolytic trimming.

RESULTS

Mapping the 5'-ends of 3'-NGD RNA fragments at single-nucleotide resolution

To generate 3'-truncated mRNA substrates for NGD *in vivo*, we inserted a hammerhead ribozyme sequence [22] in the 3'-sequence of *URA3* gene ORF (mRNA1Rz). This results in the production of an mRNA that lacks a stop codon and a polyadenylated tail, called mRNA1 in Fig. 1a and Supplementary Fig. 1a, and that is known to be an NGD target [5]. We first verified that we could detect NGD cleavages in the 3'-proximal region of mRNA1, by northern blotting with a probe corresponding to the 3'-end (probe prA, Fig. 1a and Supplementary Fig. 1a). The upstream and downstream cleavage products are referred to as 5'-NGD and 3'-NGD RNAs, respectively (Fig. 1a). We indeed detected a ladder of 3'-NGD RNA fragments in *dom34* mutant cells (Fig. 1b), in the presence or absence of active 5'-3' or 3'-5' exonucleolytic decay pathways, *i.e. xrn1* or *ski2* mutations, respectively [23]. In agreement with the current NGD model in which endonucleolytically cleaved 3'-NGD fragments are primarily degraded by the 5'-3' exoribonuclease Xrn1 [5], inactivation of the 5'-3' RNA decay pathway (*xrn1* mutant cells) produced a different ladder of 3'-NGD RNAs compared to WT or the *ski2* mutant. This was confirmed by a higher resolution PAGE analysis followed by northern blotting (Fig. 1c). The PAGE analysis was completed by mapping the 5'-ends of the 3'-NGD RNA fragments in the *dom34* and *dom34*/*xrn1* mutants by primer extension experiments with prA (Fig. 1d). We showed that the truncated mRNAs produce several discrete 3'-NGD RNA bands (B1 to B5) that can be mapped to single-nucleotide resolution. B5 (77 nts) and the major RNA species B1 (47 nts) were only detected in the presence of active 5'-3' exoribonuclease Xrn1 (Fig. 1b, 1c and 1d); B3 (68 nts) and B2 (65 nts) RNAs were exclusively observed in the *xrn1* mutant cells, and B4 (71 nts) was detected in all three strains. The sizes of the major B1 and B5 RNAs differ by 30 nts (Fig. 1d), consistent with the length of mRNA covered by an individual ribosome [24]. We therefore surmised that the difference in size is most likely due to the presence of an extra ribosome protecting the B5 RNA species from 5'-3' degradation by Xrn1, compared to B1 [25]. This prompted us to analyse the association of these 3'-NGD RNAs with ribosomes in sucrose gradients.

Ribosome association with 3'-NGD RNA fragments

We performed polysome analysis to assess the distribution of 3'-NGD RNAs in different ribosomal fractions (Supplementary Fig. 1b, 1c and 1d). As a control, we verified that the full-length mRNA1 associates with heavy polysomal fractions (≥ 3 ribosomes) (Supplementary Fig. 1e). In *dom34* mutant cells, the B1 RNA (47 nts) was found to associate with monosomes and disomes, with disomes being the theorical and optimal coverage of such a short RNA, as proposed by [9,19,26]. Indeed, the association of a 47-nt RNA species with disomes has been deduced from ribosome profiling experiments and is explained by the approximate size of the trailing ribosome protecting a full ribosome footprint (28–30 nt) and the leading ribosome protecting a half footprint to the site of mRNA truncation (16–17 nts, with no RNA or an incomplete codon in the A-site). An additional ribosome would thus be expected to protect a ~77-nt RNA. Accordingly, a portion of the B5 RNA was found to associate with three ribosomes. Although the major portion of the 71-nt B4 RNAs was associated with two ribosomes, a significant amount also associated with three ribosomes (Supplementary Fig. 1e).

We hypothesized that ribosomes do not stay stably bound to the different RNA species during sucrose gradient analysis. This prompted us to determine how these 3'-NGD RNAs were protected from Xrn1 activity in cell extracts prior to centrifugation on sucrose cushions. We first focused on the fate of the major B1 (47 nts) and B5 (77 nts) RNA species detected in *dom34* cell extracts, which likely correspond to RNAs protected from Xrn1 digestion *in vivo* by trisomes and disomes, respectively. We showed that Xrn1 treatment of RNA in *dom34* cell extracts had no impact on B5 and B1 RNAs *in vitro,* suggesting that these RNA species are indeed protected by ribosomes (Fig. 1e). Interestingly, the persistence of the 71-nt B4 RNA after Xrn1 treatment suggests that this RNA may also be protected by up to three ribosomes in the *dom34* background (Fig. 1e).

We also added purified Xrn1 to cell extracts of the *dom34*/*xrn1* strain *in vitro* and showed that it can efficiently recapitulate the production of the B1 species observed in Xrn1-containing cells *in vivo*. The appearance of the B1 RNA was inversely correlated to the amount of B4, B3 and B2 RNAs remaining, suggesting that these three species have unprotected 5'-protruding RNA extremities *in vivo,* due to the absence of the 5'-3' exoribonuclease Xrn1 (Fig. 1e). The B5 RNA was also generated at the expense of some larger species by Xrn1 treatment *in vitro*, consistent with the presence of trisomes on this species in the *dom34*/*xrn1* cell extracts (Fig. 1e). Based on these experiments, we propose that

the B1 (47 nts) and B5 (77 nts) species correspond to Xrn1-trimmed RNAs protected by two and three ribosomes, respectively [25] and that at least some portion of the 71 nt B4 RNA is also protected from Xrn1 by three ribosomes.

Ribosome protection of 3'-NGD RNA fragments from RNase I activity

To validate the presence and number of ribosomes on 3'-NGD RNAs by a third method, and particularly the presence of trisomes on the 77-nt B5 and 71-nt B4 species, we also performed RNase I protection assays on cell extracts of *dom34* and *dom34 xrn1Δ* strains. We hypothesized that B5 and B4 RNAs protected from RNase I by three ribosomes should be detectable with both probes prA and prD (Fig. 1f). The presence of two or three ribosomes on the major RNA species B1, B4 and B5 in *dom34* cells (deduced from primer extension experiments, ribosome association and Xrn1 treatment *in vitro*) would preferentially conduct RNase I to cleave at three major sites, Cut1, 2 and 3 in Fig. 1f. After RNase I treatment (Fig. 1g), the accumulation of RNase I protected RNAs of similar size to B5 is consistent with the hypothesis that this RNA is covered by trisomes in *dom34* mutant extracts (Fig. 1g). It is known that RNase I and Xrn1 cleave about 15 nts [9] and 17 nts [25] upstream of the first nt of the ribosomal A-site, respectively. We thus expected 5'-end of the B5 RNA to be 1-2 nts shorter than the Xrn1 product after RNase I treatment, if we had accurately calculated the positions of ribosomes on this RNA. Indeed, primer extension experiments confirmed that ribosomes protect a 75-nt species from RNase I in the *dom34* background (Supplementary Fig. 1f and Supplementary Fig. 1h). The equivalent of the B1 RNA was 46 nt in size after RNase I treatment (Supplementary Fig. 1i). B4 RNA was not detected using probe prA (Fig. 1g). We thus verified that RNase I cleaved preferentially at Cut3 (Fig. 1f), preventing the detection of B4 using probe prA. We then probed the membrane in Fig. 1g with prD (Fig. 1h), and two distinct RNA species were detected corresponding to B5 and B4 processed by RNase I at Cut3, and inefficiently cleaved at the Cut2 site (Fig. 1f). We thus propose that the 5'-extremities of B4 RNA are also protected by ribosomes (at least two ribosomes limiting RNase I attack at Cut2). We conducted the same experiment on the B4 RNA from *xrn1/dom34* cell extracts. These RNAs were sensitive to Xrn1 treatment *in vitro* (Fig. 1e), and using probe prD to detect the B4 RNA specifically, we observed that these RNAs were also protected from RNase I to a similar extent as B4 in *dom34* cell extracts (Fig. 1h). Thus, whether two or three ribosomes dwell on the 71-nt B4 RNA in *xrn1/dom34* mutant cell extracts is not completely clear as this species is sensitive to Xrn1 *in vitro* (*i.e.* have 5'-

ribosome-free extensions that can be pared down to B1 by Xrn1 digestions) (Fig. 1e), which would be consistent with protection by two ribosomes, but it is resistant to RNase I (Fig. 1h), which is more consistent with three. More importantly, however, these results allow us to infer the precise positions of ribosomes on B5 and B4 RNA species in the *dom34* mutant backgrounds. In this context, the above experiments all converge to the conclusion that the B5 species corresponds to RNAs covered by trisomes (Fig. 1i). We also propose that three ribosomes cover the 71-nt B4 RNA in *dom34* mutant cell extracts as this species is resistant to Xrn1 (Fig. 1e), its 5'-region is protected from RNase I digestion *in vitro* (Fig. 1h) and a significant proportion remains associated with fractions corresponding to three ribosomes in sucrose gradients, despite the suspected instability of this association under these conditions (Supplementary Fig. 1e).

The heterogeneity of 3'-NGD RNA fragments in Xrn1 deficient cells is produced by Dxo1

We strongly suspected that the B4 species was the original NGD product, and because it is exclusively detected in Xrn1 deficient cells, we speculated that the B3 and B2 RNAs might be derived from B4 by an alternative 5'-3' exoribonuclease. We therefore asked whether the 5'-3' exoribonucleolytic activity of Dxo1, which plays an important role in 5'-end capping quality control [21], might explain the presence of the B3 and B2 RNAs. Remarkably, deletion of both *xrn1* and *dxo1* genes in a *dom34* background completely abolished the production of the B3 and B2 RNAs, and only the B4 3'-NGD species remained detectable by northern blot analysis (Fig. 2a) or in primer extension assays (Supplementary Fig. 2a). Complementation of the *dom34*/*xrn1*/*dxo1* mutant with wild-type Dxo1 restored B3 and B2 RNA production to a significant extent, but a catalytic mutant failed to do so (Fig. 2b). We took advantage of the almost exclusive presence of the B4 3'-NGD RNAs in *dom34*/*xrn1*/*dxo1* mutant cells to ask how this RNA is protected by ribosomes, by adding Xrn1 to cell extracts as described above. Some of the B4 RNA was Xrn1-resistant (Supplementary Fig. 2b) in accordance with our hypothesis that a portion of this species is protected by three ribosomes in *xrn1*/*dom34* cell extracts (Supplementary Fig. 1f). Remarkably, most of the B4 RNA was degraded to a 47-nt species (Supplementary Fig. 2b),

strongly suggesting that disomes persist on the majority of the 3'-end of truncated RNAs in *dom34/xrn1/dxo1* cells *in vivo*. We thus conclude that two populations of B4 RNAs co-exist in Xrn1 deficient cells *in vivo*, with one population covered by three ribosomes, especially in *dom34* mutants, and the other only covered by two ribosomes, but having a 5'-protuding RNA extremity due to the absence of 5'-3' exoribonucleases.

We performed a number of experiments to probe the role of Dxo1 under conditions where Xrn1 is still present, but when its activity is attenuated. Inhibition of the 5'-3' exoribonuclease activity of Xrn1 occurs upon accumulation of the metabolite 3'-phospho-adenosine-5'-phosphate (pAp), for example in Met22 deficient cells, or in cells exposed to toxic levels ions such as sodium or lithium [27,28]. Remarkably, in cells containing Xrn1, the *met22* mutation or the addition of lithium led to the accumulation of B3 and B2 RNAs, while still maintaining the production of the B5 and B1 species (Fig. 2c and Supplementary Fig. 2c). Hence, Dxo1 can participate in 3'-NGD RNA trimming even under conditions where Xrn1 is still partially active.

Identification of the primary NGD endonucleolytic cleavage site

The results described above suggested that the B4 RNA is the major 3'-product of NGD cleavage in our constructs and that it is trimmed to smaller sizes by Xrn1 and Dxo1. While its resistance to Xrn1 *in vitro* (Fig. 1e) could be explained by a third ribosome dwelling after cleavage, we also considered the possibility that its 5'-phosphorylation state could contribute to its stability, since both Xrn1 and Dxo1 require 5'-phosphorylated extremities to degrade RNA [21,29]. We therefore asked whether the B4 RNA naturally has a monophosphate or a hydroxyl group at its 5'-end by treating RNA purified from *dom34* cell extracts with T4 polynucleotide kinase to see whether this would stimulate attack of B4 by Xrn1 *in vitro*. Remarkably, the B4 RNA was completely degraded by Xrn1 only after 5'-phosphorylation by T4 kinase *in vitro* (Fig. 3a), demonstrating that the B4 RNA has a 5'-OH extremity in *dom34* cells. 5'-hydroxyl and 2'-3' cyclic phosphate 3' extremities are typically generated by metal-independent endoribonucleolytic reactions [30]. It has recently been demonstrated that the Hel2 ubiquitin-protein ligase is crucial for the activation of NGD cleavages [31]. Consistent with our hypothesis that the B4 species corresponds to the 3' NGD cleavage product, this RNA is no longer produced in the *hel2* mutant (Supplementary Fig. 3a). Interestingly, the B1 and B5

NGD RNAs remain abundantly produced, confirming the important role of Xrn1 in the NGD pathway, independently of Hel2-triggered endonucleolytic cleavages.

By definition endonucleolytic cleavage of RNA results in the production of 5' and 3'-RNA fragments. However, the demonstration of their existence has never been obtained in the case of NGD targeted mRNAs. We thus searched for the corresponding 5'-NGD fragment for the B4 3'-NGD RNA. To map the 3'-end of 5'-NGD RNAs, total RNA preparations from *ski2* and *ski2*/*dom34* mutants were ligated to a pre-adenylated oligonucleotide linker using truncated RNA ligase (Fig. 3b) [32]. The *ski2* mutant context was used to limit 3'-trimming of these RNAs *in vivo*. RNAs were pre-treated with T4 polynucleotide kinase to modify 2'-3' cyclic phosphates to 3'-OH to permit RNA ligation [32]. Linker-ligated RNAs were reverse transcribed, amplified by PCR and cloned for sequencing, using a method called 3'-RNA ligase mediated RACE (called 3'-RACE below) (Fig. 3b) [33]. The major RT-PCR product was of the expected size (66 bp; Fig. 3c and Supplementary Fig. 3b) and verified by sequencing the resulting clones (Fig. 3d). The identification of a matching 5'-NGD fragment for the B4 3'-NGD RNA, confirms that an endonucleolytic event occurred at this precise position. The same procedure performed on RNAs isolated from *ski2* mutants where Dom34 is still active yielded the same major PCR product, also verified by sequence (Supplementary Fig. 3c). Thus, while the *dom34* mutation facilitates the detection of NGD fragments by increasing their stability, the cleavage event itself is Dom34-independent.

The fate of 5'-NGD RNAs

We anticipated that following NGD cleavage of mRNA1, ribosomes that had initiated translation on the 5'-NGD fragments would advance to the new 3'-end and the RNA be subjected to Xrn1 trimming, similar to the process that generates B1 and B5 (Fig. 4a). Since the B4 3'-NGD RNAs are cut in the +1 reading frame (Fig. 1h), upstream ribosomes on these 5'-NGD RNAs would be expected to stall with one nucleotide in ribosome A-site (Fig. 4a and Supplementary Fig. 4) and as result produce new RNA fragments 47+1, 77+1 nts, protected by two or three ribosomes, respectively (see Supplementary Fig. 4). Indeed, in northern blots using probe prG, which is complementary to the new 3'-ends generated by NGD cleavage, we detected RNA fragments consistent with a 1-nt increase in size compared to those detected by prA on the same membrane (Fig. 4b). We mapped the 5'-ends of these new ribosome protected fragments by primer extension assays using prG (Fig. 4c and Supplementary Fig. 4). The detection of 48-nt (and 78-nt) cDNAs only in cells containing active Xrn1 (Fig. 4c)

strongly suggests that the new NGD endonucleolytic products are covered by two and three ribosomes, respectively. The production of cDNAs of exactly the predicted sizes (48 and 78 nts) is an independent confirmation that the 3'-extremity of the 5'-NGD product corresponds precisely to the proposed NGD endonucleolytic cleavage site (Supplementary Fig. 4). Remarkably, the 3'-extremity of the 5'-NGD RNA was detected in the context of active 3'-5' exonucleases, meaning that ribosomes run on and cover the 3'-extremity before any 3'-5' attacks can occur. In summary, we propose that the B4 RNA is produced by endonucleolytic cleavage within the footprint of the third stalled ribosome and that at least two upstream ribosomes promptly protect the resulting 5'-NGD fragment from degradation (Fig. 4d).

The 5'-OH endocleaved product is phosphorylated by Rlg1/Trl1

Despite the fact that a portion of the B4 species was found to be 5'-hydroxylated in *dom34* cell extracts (Fig. 3a), the major fraction of the B4 RNA from *dom34*/*xrn1* and *dom34*/*xrn1*/*dxo1* cell extracts can be degraded by Xrn1 *in vitro* without prior 5'–phosphorylation (Fig. 1e and Supplementary Fig. 2b), suggesting that B4 accumulates as a 5'-phosphorylated species in this mutant background. A well-characterized factor with RNA kinase activity in yeast is the essential tRNA ligase Trl1, alias Rlg1 (Phizicky *et al*., 1992; Wu and Hopper, 2014). Splicing of tRNAs is known to generate 5'OH-intron RNAs which require Rlg1 kinase activity to permit their degradation by Xrn1. We therefore asked whether the 3'-NGD B4 RNA fragments were substrates of Rlg1. If Rlg1 were required for B4 degradation, loss of Rlg1 function should increase the amount of 5'-OH RNA versus 5'-P B4 RNA. Since *RLG1* is an essential gene, we used a temperature sensitive (ts) allele of *RLG1* (*rlg1-4*) for this experiment (Phizicky *et al*. 1992; Wu and Hopper, 2014). We used an *xrn1*/*dxo1*/*dom34* mutant background to focus uniquely on the B4 species (Fig. 2a and 5a). After a 3-hour shift to 37°C, RNAs isolated were analyzed on higher resolution PAGE to dissociate 5'-hydroxylated B4 RNAs from 5'-phosphorylated B4 RNAs, as previously performed to determine 5'-OH and 5'-P extremities of tRNA introns (Wu and Hopper, 2014). Upon thermo-inactivation of the *rlg1-4* allele, we observed an accumulation of the 5'-OH B4 RNA relative to the 5'-P species (Fig. 5b and Supplementary Fig. 5), consistent with this being the major kinase involved in phosphorylating the B4 RNA following NGD cleavage.

Identification of NGD cleavage products on mRNAs containing rare codons

We asked whether we could identify endonucleolytic cleavages on another NGD-targeted mRNA, using what we learned about this process on truncated mRNAs. We chose an mRNA containing four contiguous rare CGA codons, which we call $(CGA)_4$-mRNA, as an NGD target (Fig. 6a and Supplementary Fig. 6a) [5]. Similarly to the truncated mRNAs, ribosomes were shown to stall when decoding rare codons, producing 5'- and 3'-NGD RNAs (Fig. 6a). As previously demonstrated [5,34], we showed that 3'-NGD RNAs fragments can be detected in *dom34* or *DOM34* genetic contexts by northern blotting experiments using probe prB (Supplementary Fig. 6b). The precise identification of endonucleolytic cleavages by primer extension experiments is known to be challenging [5] probably because, in contrast to truncated mRNAs, the positioning of ribosomes on contiguous rare codons is variable. We first asked whether we could detect 5'-NGD RNAs (Fig. 6a) using the same procedure as for NGD-targeted truncated RNAs (Fig. 4a and 4b). By probing the $(CGA)_4$-mRNA in a large region upstream of the four CGA codons (Supplementary Fig. 6a), we detected RNA bands using a probe annealing 71 nts upstream of the first rare codon (probe prH, Fig. 6b and Supplementary Fig. 6a). Similar to the 5'-NGD RNAs produced from NGD-targeted mRNA1 (Fig. 4b), RNA detection required a *dom34* genetic background (Fig. 6b). The profile of the 5'-NGD RNAs resulting from endonucleolytic cleavages of $(CGA)_4$-mRNA were remarkably similar to B1, B4 and B5 RNAs from the truncated mRNA1. We then treated these RNAs with Xrn1 and, as anticipated, we showed that the ~71-nt RNA, like the B4 RNA, is Xrn1-resistant, and that ~47-nt and ~77-nt RNAs, like the B1 and B5 RNAs, were Xrn1-sensitive. These results strongly suggest that NGD-targeted $(CGA)_4$-mRNAs are a similar source of truncated RNAs which are, in turn, processed like mRNA1 by the NGD pathway.

The detection of short RNA species by prH probe suggested that endonucleolytic cleavages occurred just downstream, in a region located ~70 nts upstream of the cluster of rare codons (Supplementary Fig. 6a). We thus set out to map the NGD cleavage sites on the $(CGA)_4$-mRNA, using 3'-RACE for the detection of the 3'-ends of 5'-NGD RNAs in *ski2* and *ski2/dom34* mutant cells (Supplementary Fig. 6c). We obtained major RT-PCR products of about 45 bp that were purified, cloned and sequenced (Fig. 6d and Supplementary Fig. 6d). The 3'-end sequences (Fig. 6e) formed three clusters, C1, C2 and C3 (Fig. 6g), that map to ~71 nts upstream of the second, third and fourth rare codon, respectively, consistent with cleavage within the footprint of the third ribosome as seen for the truncated mRNA1. No 3'-ends were detected within the region covered by two ribosomes, comforting the notion that

disomes are not competent for NGD endonuclease activation. Xrn1 arrests mapping to 17-18 nts upstream of the A-site of the two first ribosomes positioned with either the second or third CGA codon in the A-site were also detected by primer extension assay (Fig. 6f, 6g and 6h). The strongest Xrn1 arrests corresponded to those where the lead ribosome contains the third CGA codon in the A-site (Fig. 6h), suggesting that the major stall occurs on this codon. Typically, Xrn1 is preferentially blocked 17 nts upstream of the first ribosomal A-site residue [25]. We speculate that this 1-nt difference reveals distinct conformations of stalled ribosomes on rare codons versus truncated mRNAs. All these results taken together suggest that the $(CGA)_4$-mRNA and truncated mRNA1 are NGD-targeted in a highly similar process that results in cleavage within the footprint of the third ribosome, 71 nts upstream of the stall site for the leading ribosome. As shown in Supplementary Fig. 6b, the levels of 3'-NGD RNAs produced from mRNA containing rare codons dramatically decrease in the absence of Xrn1, demonstrating that 3'-NGD RNAs resulting from endonucleolytic cleavage only represent a minor portion. This can explain why primer extension experiments principally detect Xrn1 arrests at the trailing edges of ribosomes and that 3'-RACE is more suitable for the detection of endonucleolytic cleavage sites (Fig. 6e, 6f and 6h). Cleavages have been proposed by others to occur in the region covered by disomes using primer extension experiments [5,31]. We thus analysed an mRNA containing rare codons with an identical ribosome stalling sequence to that previously examined [5] (Supplementary Fig. 6e). We demonstrate that cleavages detected in the region covered by disomes are abolished in *dxo1xrn1* mutant cells, suggesting that they are the products of subsequent trimming by these enzymes. In conclusion, our data suggests that stalled disomes on truncated mRNAs or on mRNAs containing short CGA repeats are poorly competent for NGD endonucleolytic cleavages. Endonucleolytic cleavages instead occur upstream of collided disomes, in agreement with other 3'-RACE analyses [26]. Our data suggests these cleavages first occur within the mRNA exit tunnel of the third stacked ribosome and those queuing further upstream.

Discussion

In this study, we first characterized the 3'-NGD RNA fragments produced near the 3'-end of truncated mRNAs that mimic natural cleaved mRNAs known to be NGD targets. One advantage of studying the 3'-NGD products of truncated mRNAs is that the precise positioning of stalled ribosomes results in 3'-NGD RNA fragments of specific sizes. Indeed, the precise identification of endonucleolytic cleavages is known to be challenging for mRNAs containing rare codons [5,31] probably because, in contrast to truncated mRNAs, the positioning of ribosomes on four to twelve contiguous rare codons is variable. Using a ribozyme to efficiently generate precise 3'-ends within an open reading frame, we were able to obtain detailed information about the ribosomal positioning on 3'-NGD RNAs, and provide the first precise mapping of the original site of endonucleolytic cleavage on an NGD substrate. Our model suggests that this occurs 8 nts upstream of the first P-site nt of the third ribosome stalled at the 3'-end of the truncated mRNA (Fig. 1h and Fig. 7). This localizes the cleavage within the mRNA exit tunnel, 4 nts before the RNA emerges from the ribosome and becomes available for cleavage by RNase I, classically used in ribosome foot-printing studies. This site is consistent with the idea that the NGD endonuclease might be the ribosome itself. However, we cannot fully exclude the possibility the stalled ribosome allows access to an external nuclease with a specific conformation to penetrate this far into the mRNA exit tunnel.

The NGD endonucleolytic cleavage detected within the third stalled ribosome, suggests that the first two stalled ribosomes (disome) are not competent for the activation of the endonuclease (Fig. 7). Our 3'-RACE experiments did not amplify DNA products corresponding to RNAs corresponding to the predicted sizes of NGD-cleaved RNAs with the second (41 nts) or first stalled ribosome (15 nts) (predicted sizes 95 and 125 nts, respectively), suggesting that they do not occur to any significant level. The major ~65-bp RT-PCR products obtained corresponded perfectly to RNAs cleaved 71nt upstream of the 3'-extremity of mRNA1, suggesting this is the primary site of NGD cleavage.

Xrn1 treatment of various mutant cell extracts suggested that the predominant ribosome configuration on truncated mRNAs is disomes. Interestingly, the existence of disomes on truncated mRNAs has been previously reported in ribosome profiling analysis [19] and stacking of two or more ribosomes has been proposed as a prerequisite for the activation of the endonuclease [26]. The latter observation led to the proposition that ribosome collision triggers NGD cleavage upstream of disomes. We confirm that disomes are not competent for

NGD endonuclease activation, and demonstrate that only the third or upstream ribosomes are capable of inducing cleavage. This suggests that the conformation of disomes is particular on these mRNAs and is incompatible with an NGD endonuclease activity cutting upstream of the ribosomal P-site. The ability to induce this precise NGD cleavage appears thus to be a normal property of stalled ribosomes, with disomes (and monosomes) being exceptions.

The *dom34* mutation may exaggerate the ribosome stalling and allow cleavage beyond what would naturally be observed. As discussed in the introduction, the analysis of NGD RNA fragments is facilitated by the *dom34* mutation and is crucial for RNA stabilization when analysing truncated mRNAs by northern blotting experiments [5,19]. In the presence of Dom34, and more efficient ribosome dissociation, the exosome would certainly be more actively involved once the first endonucleolytic cleavage event has occurred [5,19]. Importantly, our 3'-RACE experiments confirmed the existence of 5'-NGD products having 3'-ends matching to the 5'-extremity of the 3'-NGD B4 RNA in cells containing Dom34 (Fig. 3c and 3d). These observations were used to map endonucleolytic cleavages that occur on a second NGD-target mRNA containing rare codons, also in a *DOM34* genetic context. Endonucleolytic cleavages were mapped 71nts upstream of the first residue in the first ribosome A-site, in the region potentially covered by the third ribosome. We propose that in this case also, a particular conformation, or factor associated with disomes is responsible for their inability to trigger NGD endonuclease activity.

It has been recently reported that Cue2 is the endonuclease that cleaves NGD/NSD targeted RNAs [35,36]. Its action has been proposed to occur in the ribosomal A site and therefore deviates significantly from our observations. We do not have a good explanation for this difference. However, previous experiment with the naturally occuring truncated HAC1 mRNAs are consistent with our mapping of the endonucleolytic cleavage site [19]. The HAC1 intron is known to be excised by Ire1, but RNA ligation can be incomplete and lead to a truncated but translated mRNA [37,38]. Green and colleagues showed by ribosome profiling analysis that ribosomes stall at the 3'-end of the first exon of the HAC1 mRNA, leading to an endonucleolytic cleavage ~70 nt upstream from the 3´-end [9]. Consistent with this, our data suggests that the NGD endonuclease cleaves 71 nt upstream from the 3'-end of the truncated mRNA1 (B4 RNAs, Figure 2F and 4A). We also showed that NGD endonuclease cleaves mRNA1 in the +1 reading frame. As a consequence, upstream ribosomes run on the 5'-NGD mRNA and stall with 1 nt in the A-site. This is in agreement with ribosome profiling analysis

reporting the predominance of short RNAs having one 3'-nucleotide in the ribosomal A site [19,35]

Our experiments also show that the NGD endonuclease produces downstream cleavage products bearing a 5'-hydroxyl group (Fig. 3a), typical of cleavage reactions not involving a metal ion. We show that the Rlg1/Trl1 kinase, in addition to its role in tRNA splicing, phosphorylates the 3'-NGD fragment to allow degradation by Xrn1 and Dxo1 (Fig. 5b and Supplementary Fig. 5). The resistance of the 3'-NGD B4 RNA fragments to Xrn1 attacks *in vitro* and *in vitro* (Fig. 1e) is likely to be a direct consequence of the presence of the third ribosome preventing access to Rlg1/Trl1. Accordingly, the extremities of the B4 RNAs were shown to be mostly 5' hydroxylated in an *XRN1/dom34* context, while an important portion of B4 RNAs were 5'-monophosphorylated in *dom34/xrn1* and *dom34/xrn1/dxo1* mutant cell extracts, where these RNAs accumulate in the absence of Xrn1 and are mostly associated with disomes. An important conclusion is that Rlg1 is a far more general RNA kinase than previously suspected, and acts in the NGD pathway. Rlg1 was also recently shown to phosphorylate a 5'-hydroxylated exon of the HAC1 mRNA to facilitate its digestion by Xrn1 [39]. Another conclusion is that NGD endonucleolytic cleavage does not randomly occur upstream of the ribosomal stall site and is not an artefact of *dom34* genetic context. It can be precisely mapped as a unique cleavage event within the ribosomal mRNA exit tunnel 8 nt upstream of the first P-site residue. Remarkably, mRNAs containing rare codons are processed similarly, but cleavage accuracy is slightly affected and might be explained by a particular conformation of the first stalled ribosome [31] that correlates with specific Xrn1 arrests (Fig. 6f). Ribosomal A-site and occupancy of the mRNA entrance tunnel by mRNAs containing rare codons could thus explain some of the minor differences observed with truncated mRNAs. We also learned that the inactivation of Xrn1 can lead to a Dxo1 trimming that can mask the original cleavage event and scramble global analysis. In conclusion, this study provides very important new mechanistic insights that will help to go further in the comprehension of all mRNA surveillance pathways in connection to NGD.

REFERENCES

1 Doma, M. K. & Parker, R. Endonucleolytic cleavage of eukaryotic mRNAs with stalls in translation elongation. Nature 440, 561-564 (2006).

2 Passos, D. O. et al. Analysis of Dom34 and its function in no-go decay. Mol Biol Cell 20, 3025-3032 (2009).

3 Chen, L. et al. Structure of the Dom34-Hbs1 complex and implications for no-go decay. Nat Struct Mol Biol 17, 1233-1240 (2010).

4 Letzring, D. P., Dean, K. M. & Grayhack, E. J. Control of translation efficiency in yeast by codon-anticodon interactions. RNA 16, 2516-2528 (2010).

5 Tsuboi, T. et al. Dom34:hbs1 plays a general role in quality-control systems by dissociation of a stalled ribosome at the 3' end of aberrant mRNA. Mol Cell 46, 518-529 (2012).

6 Simms, C. L., Hudson, B. H., Mosior, J. W., Rangwala, A. S. & Zaher, H. S. An active role for the ribosome in determining the fate of oxidized mRNA. Cell reports 9, 1256-1264 (2014).

7 Sinturel, F. et al. Cytoplasmic Control of Sense-Antisense mRNA Pairs. Cell reports 12, 1853-1864 (2015).

8 Simms, C. L., Thomas, E. N. & Zaher, H. S. Ribosome-based quality control of mRNA and nascent peptides. Wiley interdisciplinary reviews. RNA 8, doi:10.1002/wrna.1366 (2017).

9 Guydosh, N. R. & Green, R. Translation of poly(A) tails leads to precise mRNA cleavage. RNA 23, 749-761 (2017).

10 Frischmeyer, P. A. et al. An mRNA surveillance mechanism that eliminates transcripts lacking termination codons. Science 295, 2258-2261 (2002).

11 van Hoof, A., Frischmeyer, P. A., Dietz, H. C. & Parker, R. Exosome-mediated recognition and degradation of mRNAs lacking a termination codon. Science 295, 2262-2264 (2002).

12 Kuroha, K. et al. Receptor for activated C kinase 1 stimulates nascent polypeptide-dependent translation arrest. EMBO Rep 11, 956-961 (2010).

13 Brandman, O. et al. A ribosome-bound quality control complex triggers degradation of nascent peptides and signals translation stress. Cell 151, 1042-1054 (2012).

14 Defenouillere, Q. et al. Cdc48-associated complex bound to 60S particles is required for the clearance of aberrant translation products. Proc Natl Acad Sci U S A 110, 5046-5051 (2013).

15 Shen, P. S. et al. Protein synthesis. Rqc2p and 60S ribosomal subunits mediate mRNA-independent elongation of nascent chains. Science 347, 75-78 (2015).

16 Johnson, A. W. & Kolodner, R. D. Synthetic lethality of sep1 (xrn1) ski2 and sep1 (xrn1) ski3 mutants of Saccharomyces cerevisiae is independent of killer virus and suggests a general role for these genes in translation control. Mol Cell Biol 15, 2719-2727 (1995).

17 Shoemaker, C. J., Eyler, D. E. & Green, R. Dom34:Hbs1 promotes subunit dissociation and peptidyl-tRNA drop-off to initiate no-go decay. Science 330, 369-372 (2010).

18 Guydosh, N. R., Kimmig, P., Walter, P. & Green, R. Regulated Ire1-dependent mRNA decay requires no-go mRNA degradation to maintain endoplasmic reticulum homeostasis in S. pombe. eLife 6, doi:10.7554/eLife.29216 (2017).

19 Guydosh, N. R. & Green, R. Dom34 rescues ribosomes in 3' untranslated regions. Cell 156, 950-962 (2014).

20 Wu, J. & Hopper, A. K. Healing for destruction: tRNA intron degradation in yeast is a two-step cytoplasmic process catalyzed by tRNA ligase Rlg1 and 5'-to-3' exonuclease Xrn1. Genes Dev 28, 1556-1561 (2014).

21 Chang, J. H. et al. Dxo1 is a new type of eukaryotic enzyme with both decapping and 5'-3' exoribonuclease activity. Nat Struct Mol Biol 19, 1011-1017 (2012).

22 Eckner, R., Ellmeier, W. & Birnstiel, M. L. Mature mRNA 3' end formation stimulates RNA export from the nucleus. The EMBO journal 10, 3513-3522 (1991).

23 Parker, R. RNA degradation in Saccharomyces cerevisae. Genetics 191, 671-702 (2012).

24 Ingolia, N. T., Ghaemmaghami, S., Newman, J. R. & Weissman, J. S. Genome-wide analysis in vivo of translation with nucleotide resolution using ribosome profiling. Science 324, 218-223 (2009).

25 Pelechano, V., Wei, W. & Steinmetz, L. M. Widespread Co-translational RNA Decay Reveals Ribosome Dynamics. Cell 161, 1400-1412 (2015).

26 Simms, C. L., Yan, L. L. & Zaher, H. S. Ribosome Collision Is Critical for Quality Control during No-Go Decay. Mol Cell 68, 361-373 (2017).

27 Dichtl, B., Stevens, A. & Tollervey, D. Lithium toxicity in yeast is due to the inhibition of RNA processing enzymes. The EMBO journal 16, 7184-7195 (1997).

28 Todeschini, A. L., Condon, C. & Benard, L. Sodium-induced GCN4 expression controls the accumulation of the 5' to 3' RNA degradation inhibitor, 3'-phosphoadenosine 5'-phosphate. J Biol Chem 281, 3276-3282 (2006).

29 Nagarajan, V. K., Jones, C. I., Newbury, S. F. & Green, P. J. XRN 5'-->3' exoribonucleases: structure, mechanisms and functions. Biochim Biophys Acta 1829, 590-603 (2013).

30 Gonzalez, T. N., Sidrauski, C., Dorfler, S. & Walter, P. Mechanism of non-spliceosomal mRNA splicing in the unfolded protein response pathway. The EMBO journal 18, 3119-3132 (1999).

31 Ikeuchi, K. et al. Collided ribosomes form a unique structural interface to induce Hel2-driven quality control pathways. The EMBO journal 38, doi:10.15252/embj.2018100276 (2019).

32 McGlincy, N. J. & Ingolia, N. T. Transcriptome-wide measurement of translation by ribosome profiling. Methods 126, 112-129 (2017).

33 Adkar-Purushothama, C. R., Bru, P. & Perreault, J. P. 3' RNA ligase mediated rapid amplification of cDNA ends for validating viroid induced cleavage at the 3' extremity of the host mRNA. Journal of virological methods 250, 29-33 (2017).

34 Chen, H. & Xiong, L. The bifunctional abiotic stress signalling regulator and endogenous RNA silencing suppressor FIERY1 is required for lateral root formation. Plant Cell Environ 33, 2180-2190 (2010).

35 D'Orazio, K. N. et al. The endonuclease Cue2 cleaves mRNAs at stalled ribosomes during No Go Decay. eLife 8, doi:10.7554/eLife.49117 (2019).

36 Glover, M. L. et al. NONU-1 encodes a conserved endonuclease required for mRNA translation surveillance. bioRxiv 674358; doi: https://doi.org/10.1101/674358 (2019).

37 Cox, J. S. & Walter, P. A novel mechanism for regulating activity of a transcription factor that controls the unfolded protein response. Cell 87, 391-404 (1996).

38 Harigaya, Y. & Parker, R. Global analysis of mRNA decay intermediates in Saccharomyces cerevisiae. Proc Natl Acad Sci U S A 109, 11764-11769 (2012).

39 Cherry, P. D., Peach, S. E. & Hesselberth, J. R. Multiple decay events target HAC1 mRNA during splicing to regulate the unfolded protein response. eLife 8, doi:10.7554/eLife.42262 (2019).

40 Anand, R., Beach, A., Li, K. & Haber, J. Rad51-mediated double-strand break repair and mismatch correction of divergent substrates. Nature 544, 377-380 (2017).

41 Mumberg, D., Muller, R. & Funk, M. Yeast vectors for the controlled expression of heterologous proteins in different genetic backgrounds. Gene 156, 119-122 (1995).

Author contributions:

A.N., S.C., R.S.F., J.H., C.T. and L.B. designed, performed and analysed data. L.B. wrote the manuscript.

Acknowledgements

This work has been supported by AAP Emergence Sorbonne Université, SU-16-R-EMR-03 and by the "Initiative d'Excellence" program from the French State grant "DYNAMO", ANR-11-LABX-0011-01. S.C. was a recipient of fellowship from the Ministère pour la Recherche et la Technologie (MNRT). A.N. was supported by a doctoral grant from "DYNAMO", ANR-11-LABX-0011-01. We thank Eric Phizicky and Anita Hopper for providing *rgl1-4* mutant and derivative strains. We thank Ciaran Condon, Josette Banroques and Kyle Tanner for technical assistance. We thank Ciaran Condon for comments on the manuscript and constructive discussions.

Competing financial interests statement.

The authors declare no competing financial interests.

End notes:

Additional Information: this manuscript contains Supplementary Information, 6 Supplementary Figures and 4 Supplementary Tables.

Fig.1

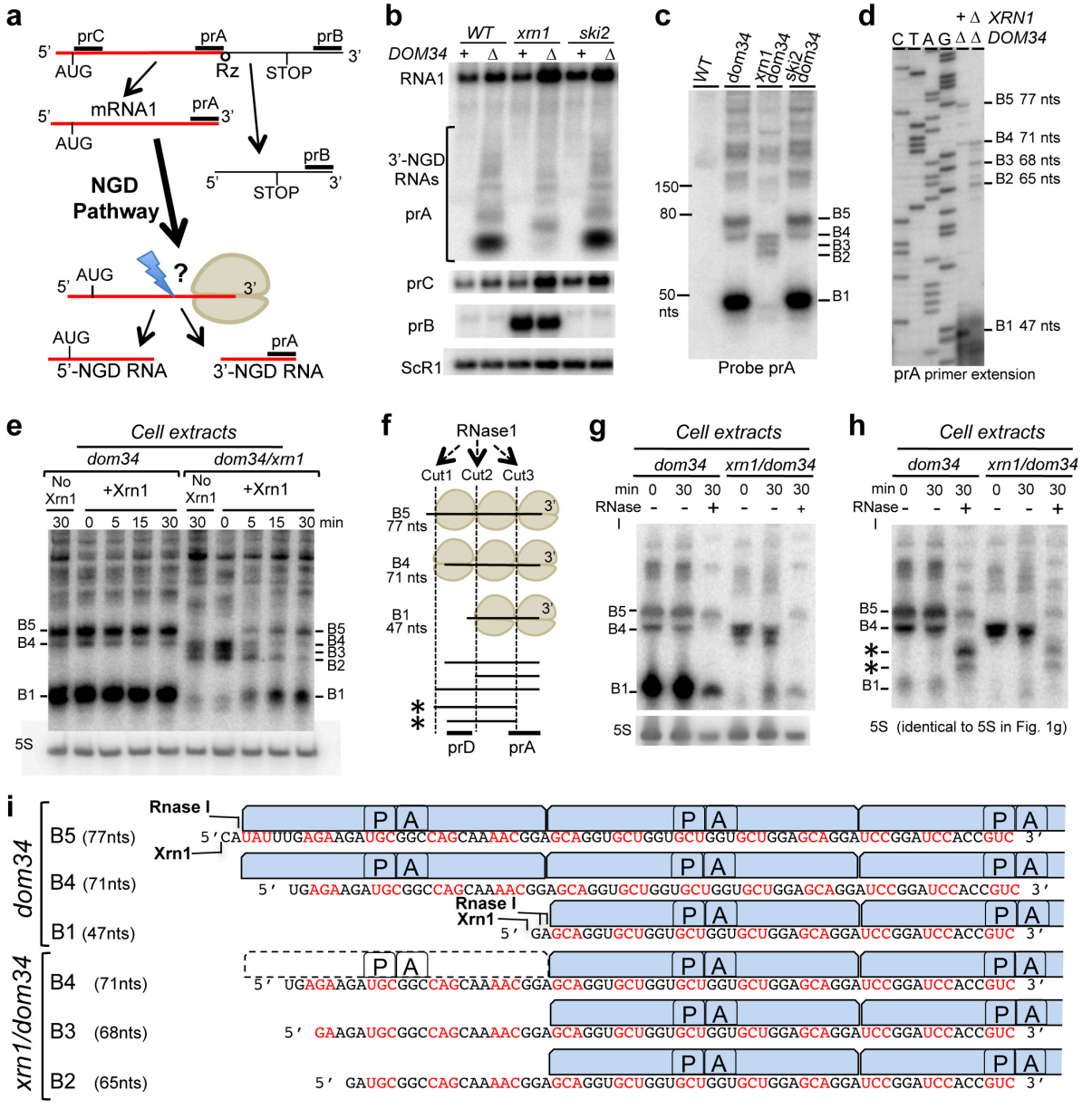

Fig.1: Size characterization of 3'-NGD RNA fragments at single nucleotide resolution and RNase ribosomal protection assay (a) Schematic view of the URA3Rz mRNA showing the ribozyme (Rz) site (see detailed sequence in Supplementary Fig. 1a). Translational start (AUG) and stop codons are indicated. RNA1 (in red) is the truncated stop-codon-less mRNA following ribozyme cleavage (see also Supplementary Fig. 1a). Probes prA, prB and prC used in northern blots analysis are indicated. 5' and 3'-NGD RNAs are the resulting products of NGD cleavage of mRNA1. The lightning flash represents the NGD endonucleolytic cleavage upstream of the ribosome stall site and probe prA is designed for the detection of all potential 3'-NGD RNAs (see also Supplementary Fig. 1a) **(b)** Agarose gel electrophoresis followed by northern blot showing steady state levels of RNA (mRNA1 and 3'-NGD RNA fragments) in wild-type and the indicated mutant strains. The scR1 RNA served as a loading control **(c)** 8% PAGE followed by northern blot analysis using probe prA showing steady state levels of 3'-NGD RNA in the indicated mutant strains **(d)** Primer extension experiments using probe prA to determine the 5'-end of 3'-NGD RNAs. B1, B2, B3, B4 and B5 RNAs shown in Fig. 1c are indicated with the corresponding size calculated by primer extension. **(e)** Xrn1 treatment *in*

vitro of cell extracts (*i.e.* mRNAs in presence of ribosomes) from *dom34* or mutant cells, followed by RNA extraction and northern blot using probe prA. Sizes in nts are deduced from experiments (**c**) and (**d**). (**f**) Schematic view of ribosomes covering RNA species B1, B4 and B5 observed in *dom34* mutant cells. Cut1, Cut2 and Cut3 represent potential RNase I cleavage sites. Probes prA and prD used in northern blots analysis shown in (**g**) and (**h**) are indicated. 5'-extremities of B5 and B4 RNAs potentially protected by two ribosomes and detected by prD are indicated by asterisks. (**g**) RNase I treatment of cell extracts *in vitro*, analysed as in (**e**). (**h**) The same membrane in (**g**) has been probed with prD. (**i**) Schematic view of the ribosome positioning on 3'-NGD RNAs combining information about single-nucleotide size resolution, ribosomal association, and Xrn1 or RNase I ribosomal protection of 3'-NGD RNAs. ORF codons are shown in black or red. A and P are ribosomal A- and P-sites respectively.

Fig. 2

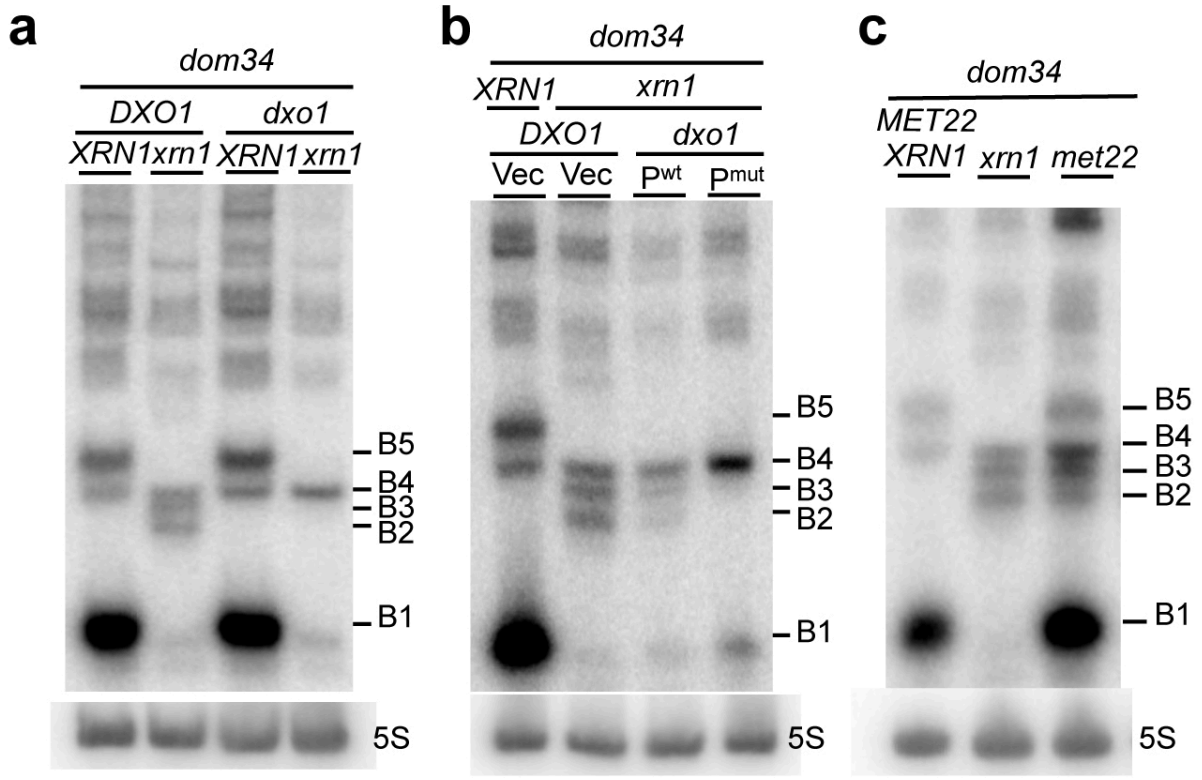

Fig. 2: Dxo1 creates the heterogeneity of 3'-NGD RNA fragments in Xrn1 deficient cells. 8% PAGE followed by northern blot analysis using probe prA showing steady state levels of RNAs in *dom34* and other indicated mutant strains. The 5S rRNA served as a loading control **(a)** Impact of *DXO1* deletion on B2 and B3 RNA production. (**b**) Plasmid expression of wild-type Dxo1 (P^{wt}) or a Dxo1 catalytic mutant (P^{mut}) (mutant E260A/D262A) [21]. The vector control is plasmid pRS313 (Vec). (**c**) Detection of B2 and B3 RNAs under conditions of partial Xrn1 inhibition in *met22* mutant strain.

Fig. 3

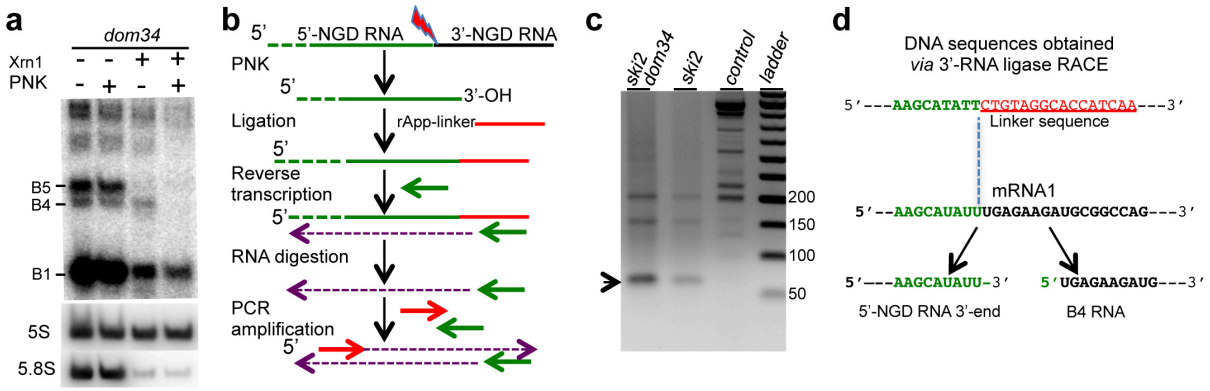

Fig. 3: Characterization of the endonucleolytic RNA fragments. (**a**) Xrn1 digestion of total RNA extracts from *dom34* mutant cells in the presence or absence of T4 polynucleotide kinase *in vitro*. 8% PAGE followed by northern blot analysis using probe prA. The 5S rRNA served as a loading control and 5.8S rRNA as a positive control of Xrn1 treatment (**b**) Flow chart illustrating the method used for 3'-end mapping, called 3'-RNA ligase mediated RACE as described in [33] with minor modifications according to [32] (see experimental procedures). (**c**) PCR products obtained from 3'-RACE and migrated on 2% agarose gel. Purified DNAs for sequencing are indicated by an arrowhead. Prior to PCR, cDNAs were produced from total RNA from *ski2*, *ski2*/*dom34* mutant cells expressing mRNA1. Control is made of total RNA from *ski2*/*dom34* mutant cells without mRNA1 expression. (**d**) Sequences obtained after 3'-RACE performed on *ski2* and *ski2*/*dom34* total RNA. 100% of sequenced clones (omitting a residual 5S rRNA-linker amplification detected) have this DNA sequence. 5'-NGD DNA sequence (in green) and linker sequence (in red). Below, the site of mRNA1 is shown before and after the cleavage producing the 3'-NGD RNA B4 and the 3'-extremity of the 5'-NGD RNA confirmed by 3'-RACE.

Fig. 4

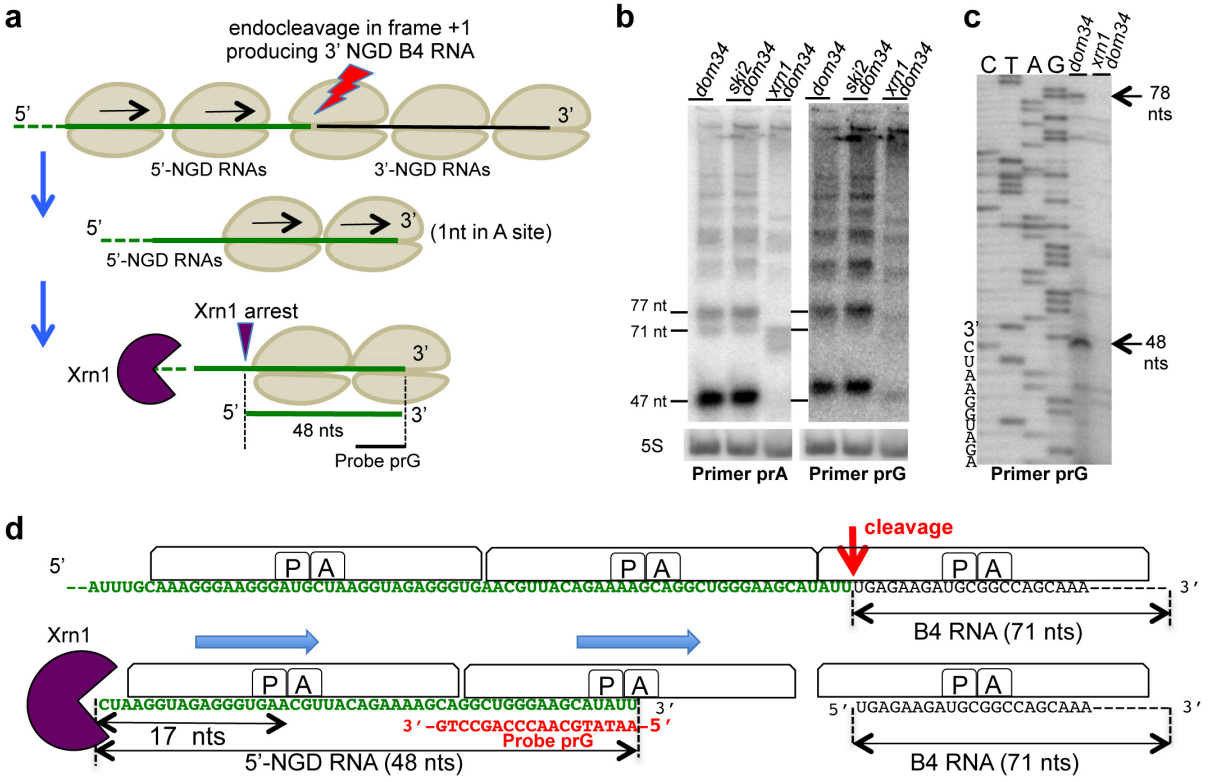

Fig. 4: Analysis of the fate of 5'-NGD RNAs. (**a**) Schematic model of mRNA1 before and after the endonucleolytic cleavages producing B4 RNAs. 5'-NGD resulting RNAs are shown here covered by two ribosomes and processed by Xrn1 to 48-nt RNAs (see also Supplementary Fig. 4 for 5'-NGD RNAs covered by three ribosomes). (**b**) 8% PAGE followed by northern blot analysis using probe prG showing steady state levels of RNAs in the indicated mutant strains (left panel). Same membrane has been probed with prA as a ladder (right panel), and sizes of B5 (77nt), B4 (71 nt) and B1 (47nt) are indicated. The 5S rRNA served as a loading control. **(c)** Primer extension experiments using probe prG to determine the 5'-end of RNAs (see also Supplementary Fig. 5). (**d**) Schematic model of ribosome positioning on mRNA1 before and after the unique endonucleolytic cleavage producing B4 RNAs, localized 8 nts upstream of the first P-site nt. The position of disomes on the resulting 48-nt 5'-NGD RNA is shown with the distal ribosome having 1 nt in the A site (see also Supplementary Fig. 4).

Fig. 5

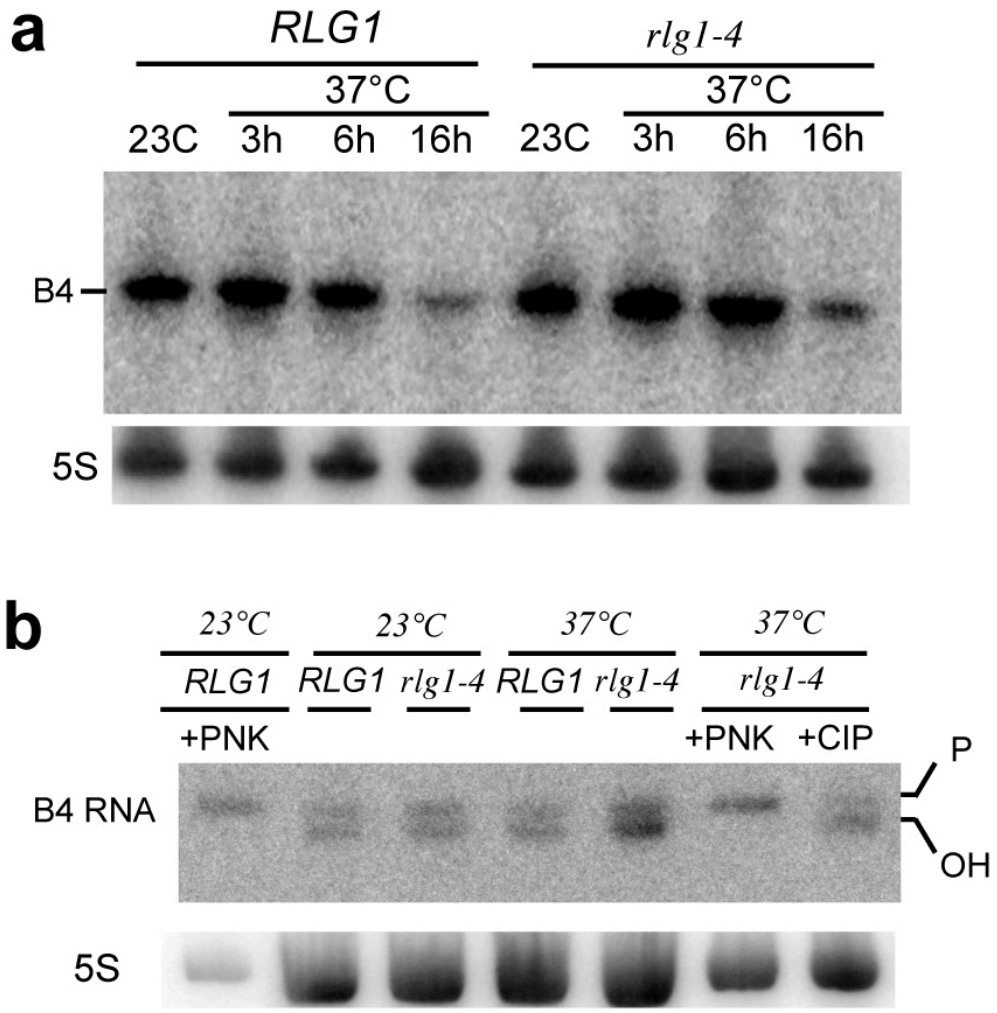

Fig. 5: Endonucleolytically cleaved 5'-OH RNAs are phosphorylated by Rlg1/Trl1. (**a**) 8% PAGE followed by northern blot analysis using probe prA. Levels of 3'-NGD RNA fragments in *rlg1-4/xrn1/dxo1/dom34* cells compared with those from *RLG1/xrn1/dxo1/dom34* cells at 23°C and after a shift to the non-permissive temperature (37°C) for 3, 6 and 16 hours. (**b**) 12% PAGE followed by northern blot analysis using probe prA. 5'-OH and 5'-P B4 RNAs from the indicated strains were separated. Treatment using Polynucleotide kinase (PNK) of total RNA from *RLG1* strain (grown at 23°C) and PNK treatment and phosphatase (CIP) of RNA from *rlg1-4* mutant strains shift at 37°C determine 5'-OH and 5'-P B4 RNA positions. The 5S rRNA served as a loading control.

Fig. 6

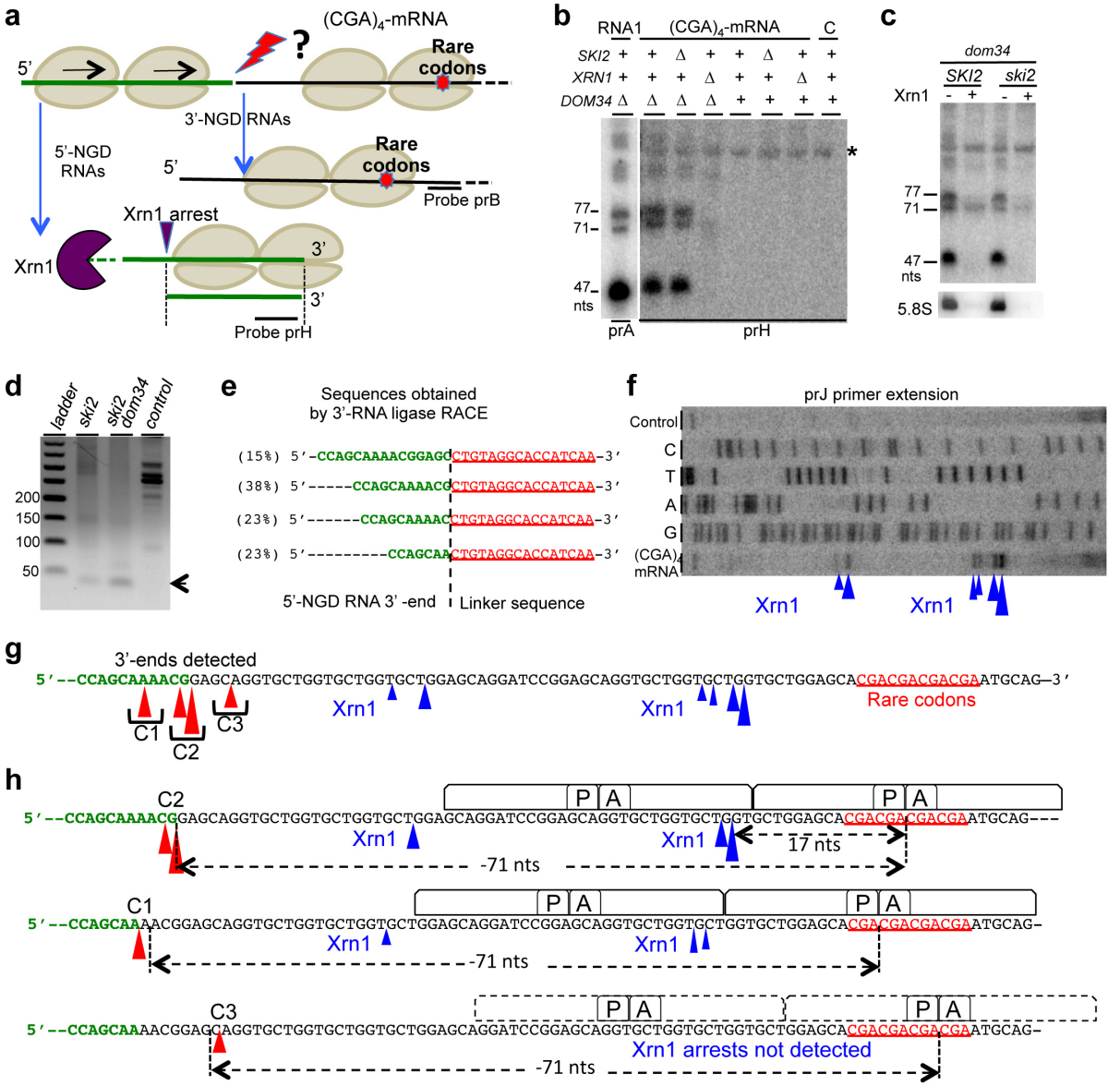

Fig. 6: identification of the endonucleolytic cleavages on the NGD targeted $(CGA)_4$-mRNA. (a) Schematic view of the $(CGA)_4$-mRNA. 5'- and 3'-NGD RNAs are the expected products of NGD. The lightning flash represents the potential endonucleolytic cleavage upstream of the ribosome stall site. Probes prB and prH are indicated. 5'-NDG RNAs are shown potentially processed by Xrn1 as described in Fig. 4a, 4d and Supplementary Fig. 4. **(b)** 8% PAGE followed by northern blot analysis using probe prH showing steady state levels of RNAs in the indicated mutant strains. Same membrane has been probed with prA as a ladder, and sizes of mRNA1 products such as B5 (77nt), B4 (71 nt) and B1 (47nt) are indicated. Only the *dom34* lane is shown. See Supplementary Fig. 6a for the sequence probed by prH. The 5S rRNA served as a loading control. Total RNA from WT cells without $(CGA)_4$-mRNA expression served as a control, noted C. A non-specific band is indicated by an asterisk. (**c**) Xrn1 treatment *in vitro* of total RNA from *dom34* or *dom34*/*ski2* mutant cells and northern blot using probe prH. The 5.8S rRNA is a positive control of Xrn1 treatment **(d)** PCR products obtained from 3'-RNA ligase mediated RACE (see also Fig. 3c). Prior to PCR, cDNAs were produced from cells expressing $(CGA)_4$-mRNA. Total RNA from cells without $(CGA)_4$-mRNA expression served as a control. (**e**) Sequences obtained after 3'-RACE

performed in (d) on *ski2*/*DOM34* total RNA. Sequence distribution is given in percentage. (**f**) Primer extension experiments using probe prJ to determine the 5'-end of RNAs. Xrn1-specific arrests are indicated by arrowheads. (**g**) Positioning of 3'-ends detected by 3'-RACE on $(CGA)_4$-mRNA from *ski2*/*DOM34* cells (red arrowhead). Arrowhead sizes are proportional to the relative number of sequences obtained. Three cleavage clusters, C1, C2 and C3 were defined (see also Supplementary Fig. 6d). Xrn1 arrests deduced from primer extension (**f**) are indicated by black arrowhead with sizes proportional to the intensity of reverse stops observed in (**f**). (**h**) Schematic view of the ribosome positioning on $(CGA)_4$-mRNA deduced from Xrn1 arrests combined with the positioning of endonucleolytic cleavages provided by 3'-RACE.

Fig. 7

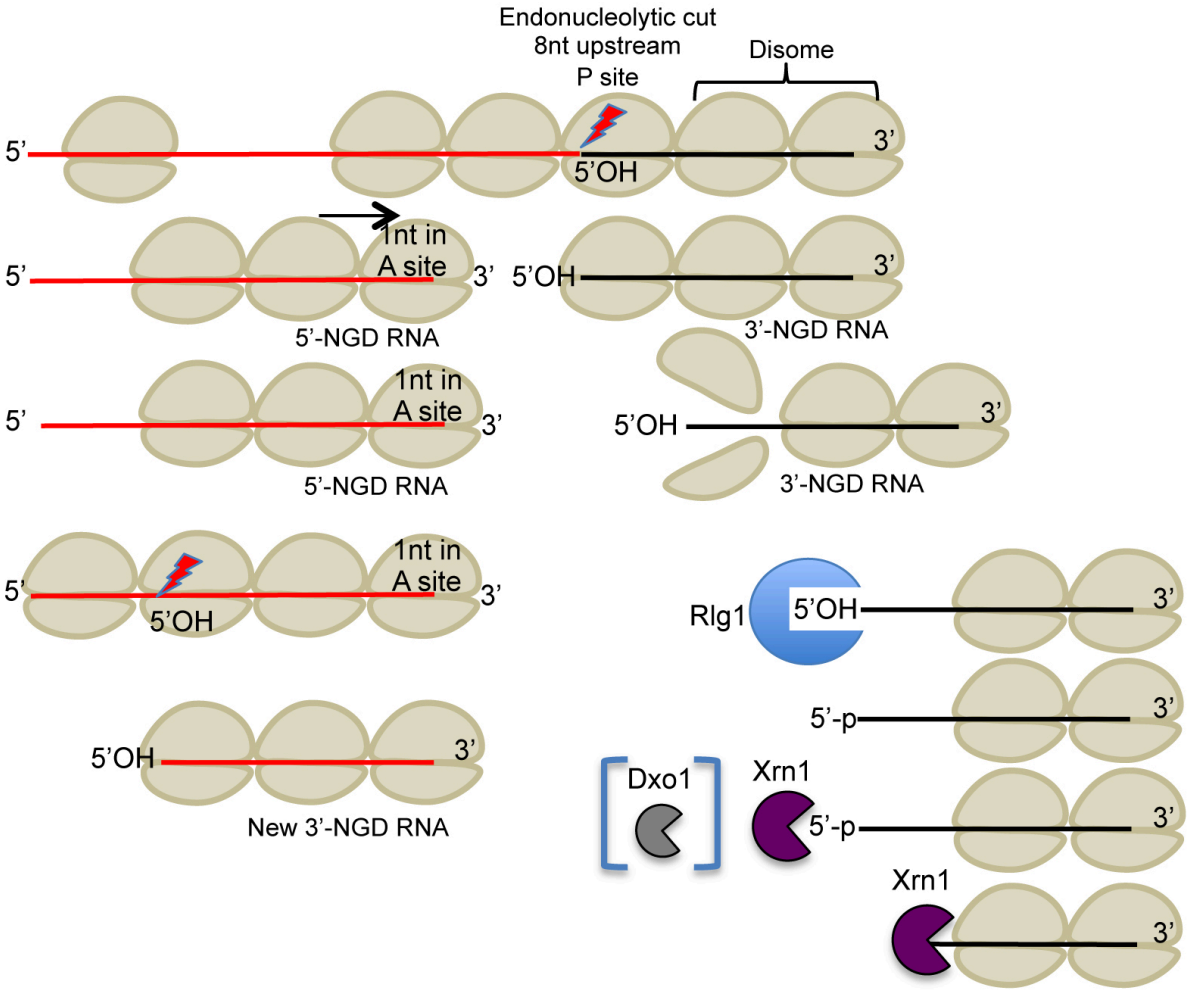

Fig. 7: Model of No-Go decay pathway involving NGD endonuclease cleavage within ribosomal mRNA exit tunnel, Rlg1 kinase and 5'-3' exoribonucleases. Here, the third ribosome is represented as competent for NGD endonuclease activation, but upstream ribosomes are also competent. We propose that the two first stalled ribosomes are not properly conformed to trigger the endonucleolytic process. NGD endonuclease cleavage (lightning flash) occurs 8 nts upstream of the first P-site residue, within the mRNA exit tunnel of the ribosome. Upstream ribosomes covering the resulting 5'-NGD fragments can advance and stall on the new 3'-end with 1 nt in the ribosomal A-site. Colliding ribosomes on this new RNA fragment can induce a novel NGD endonuclease activation. After endonucleolytic cleavage, the NGD-competent ribosome dissociates and facilitates access of Rlg1 RNA kinase to the 5'-hydroxylated 3'-NGD RNA. Once the RNA is 5'-phosphorylated, the processive 5'-3' exonucleolytic activity of Xrn1 can degrade, or alternatively, 5'-3' exonucleolytic digestion of this RNA by Dxo1 can occur.

Supplementary Fig. 1

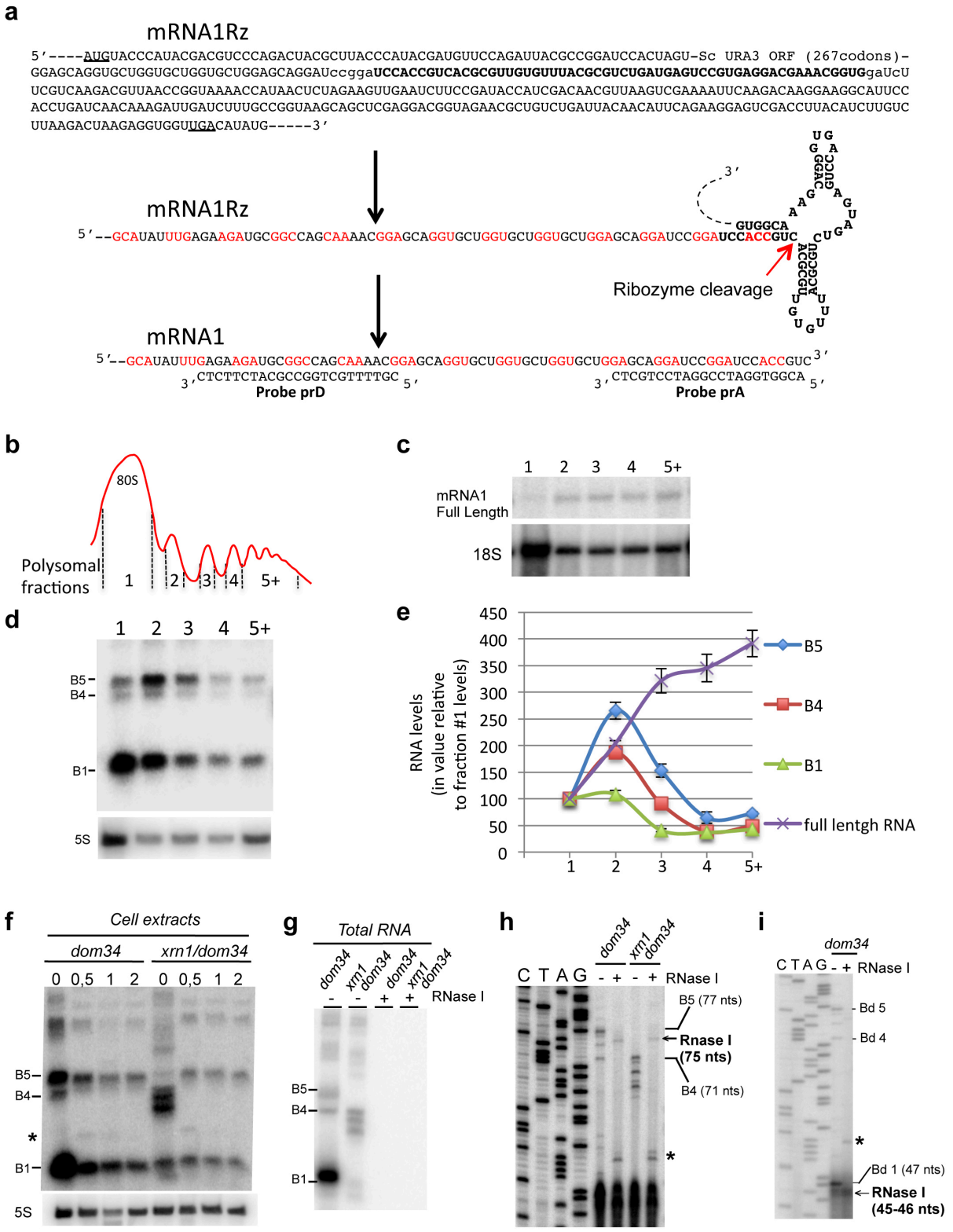

Supplementary Fig. 1: 3'-NGD RNA fragment analysis, related to Fig. 1. **(a)** Sequence of mRNA1Rz. The translational start (AUG) and stop codon (UGA) are underlined. The ribozyme sequence is shown in bold. The arrow indicates the ribozyme cleavage site. mRNA1 is the truncated stop-less codon mRNA after ribozyme cleavage. Probes prA and prD are indicated. **(b)** Representation of polysomal fractions corresponding to 1, 2, 3, 4 and ≥ 5 ribosomes (noted 5+) collected and from which RNA was extracted (see Experimental

Procedures). **(c)** 1.4% agarose gel followed by northern blot showing steady state levels of full length mRNA1. **(d)** 8% PAGE followed by northern blotting analysis using probe prA for the detection of B1, b4 and B5 3'-NGD RNA fragments. **(e)** Plot representing the potential association of 3'-NGD RNAs to ribosomes in *dom34* mutant cells. Polysomal fractions corresponding to 1, 2, 3, 4 and ≥ 5 ribosomes (noted 5+) are indicated. B5, B4 or B1 RNA quantifications were standardized using 5S rRNA. Full length mRNA1 quantifications were standardized using 18S rRNA. For each fraction, levels of RNAs were plotted as a % relative to RNA amount calculated in the first fraction (monosomal fraction). All quantifications are indicated with standard errors calculated from at least three independent experiments. (**f**) RNase I treatment *in vitro* of cell extracts (*i.e* mRNAs in presence of ribosomes) from *dom34* or *dom34*/*xrn1* mutant cells followed northern blot using probe prA. The 5S rRNA served as a loading control. **(g)** Similar RNase I treatment analysis that in (**f**) but I on extracted RNAs (*i.e* mRNAs in absence of ribosomes). **(h)** and (**i**) Primer extension experiments using probe prA to determine the 5'-end of RNAs after RNase I treatment of *dom34* and *xnr1*/*dom34* cell extracts as performed in (**f**). The band indicated by an asterisk is lost at a higher concentration of RNase I as shown in (**f**).

Supplementary Fig. 2

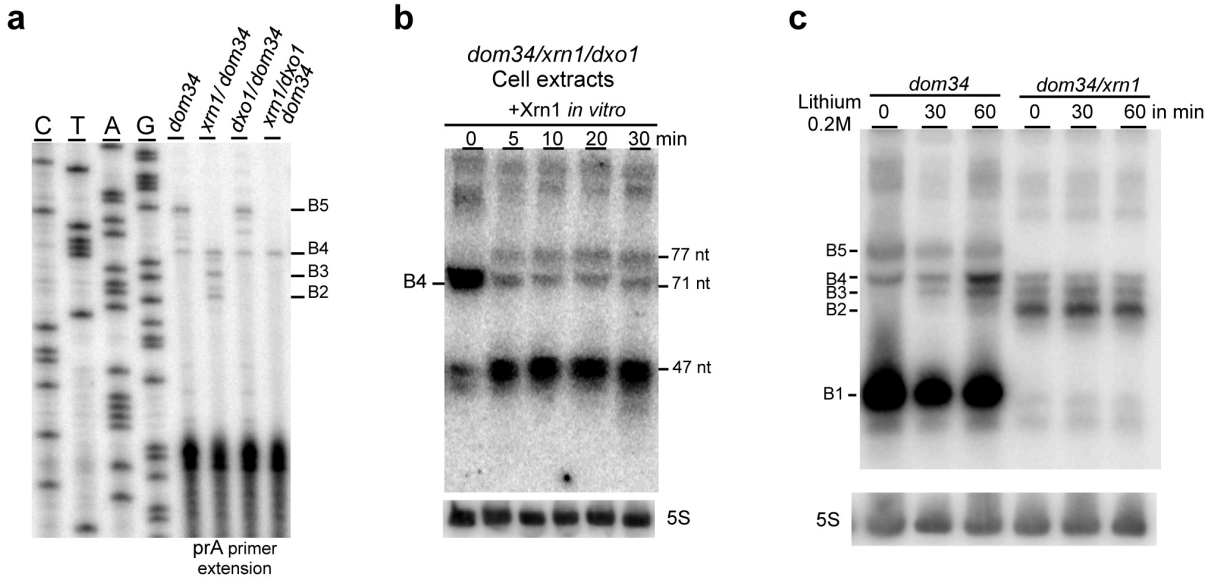

Supplementary Fig. 2: Dxo1 produces heterogeneity of 3'-NGD RNA fragments in Xrn1 deficient cells, related to Fig. 3. (**a**) Primer extension experiments using probe prA for determining the 5'-end of B1, B2, B3, B4 and B5 3'-NGD RNAs in indicated strains. **(b)** Cell extracts from *xrn1/dxo1/dom34* cells are digested by Xrn1 *in vitro*. 8% PAGE followed by northern blotting analysis using probe prA. **(c)** Effect of lithium on 3'-NGD RNA levels. 8% PAGE followed by northern blotting analysis showing levels of 3'-NGD RNAs in indicated strains.

Supplementary Fig. 3

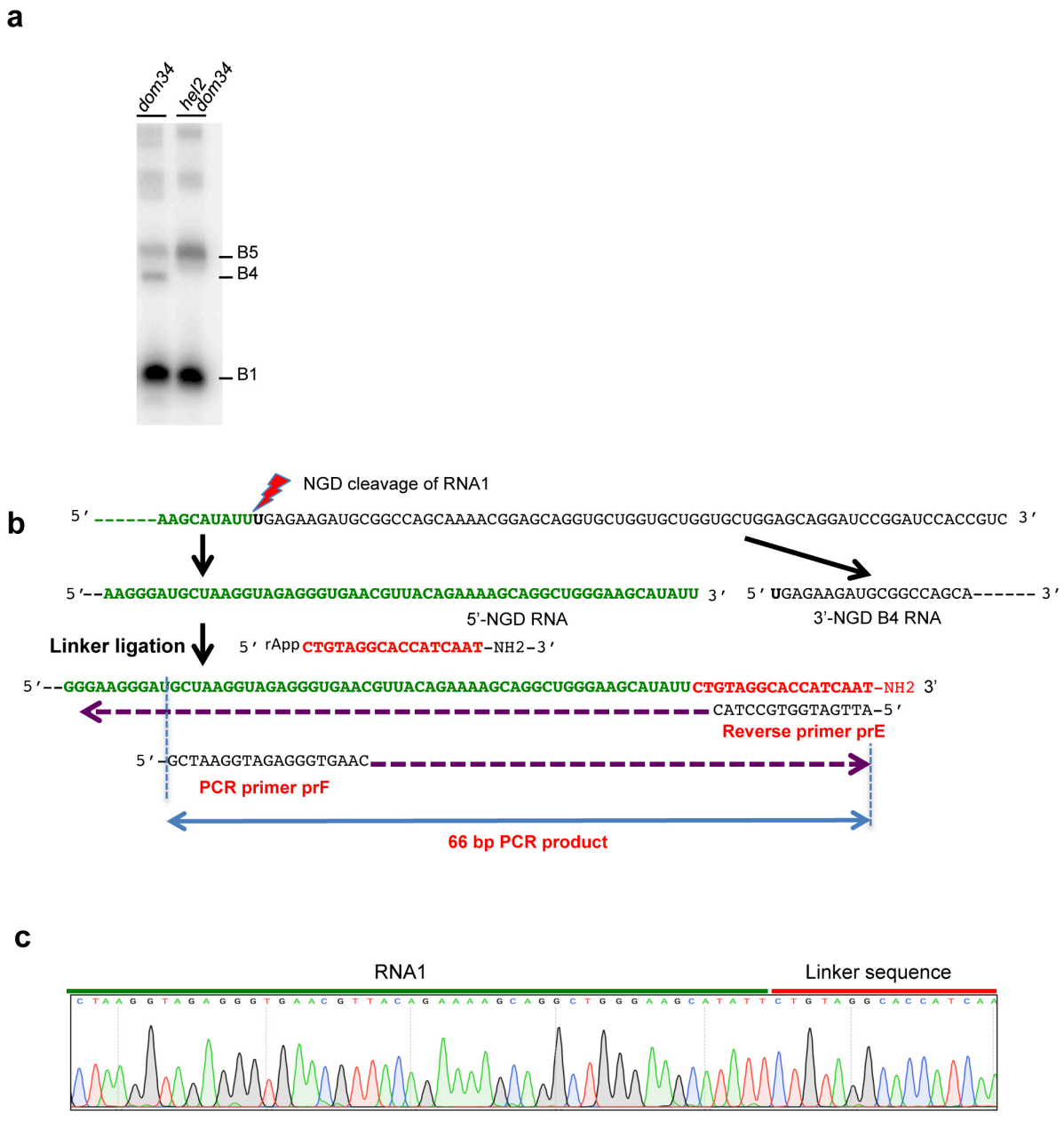

Supplementary Fig. 3: Characterization of B4 RNAs and 3'-RNA ligase mediated RACE, related to Fig. 3. **(a)** B4 RNA production is not detected in *hel2dom34* mutant cells. 8% PAGE followed by northern blotting analysis using probe prA. **(b)** mRNA1 before and after the endonucleolytic cleavage (represented by the lightning flash) producing the 3'-NGD B4 RNA, and the resulting 5'-NGD RNA. The expected 3'-extremity is shown ligated to the universal miRNA linker. Sequence of reverse primer prE and PCR primer prF are indicated. A PCR product of 66bp is expected. (**c**) Chromatogram representing sequences obtained from 3'-RACE experiments performed on total RNA from *ski2* and *ski2*/*dom34* mutant cells.

Supplementary Fig. 4

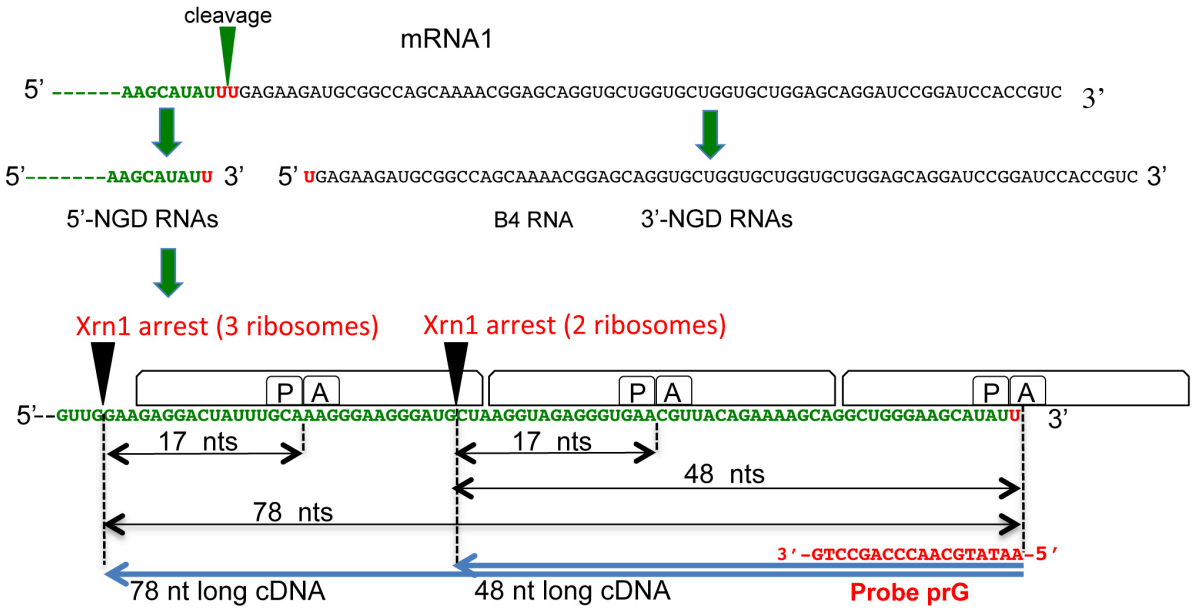

Supplementary Fig. 4: Analysis of the fate of 5'-NGD RNA, related to Fig. 4. Schematic model of mRNA1 before and after the endonucleolytic cleavage producing B4 RNA. The 5'-NGD resulting RNA is shown covered by ribosomes and is shown processed by Xrn1 in 48- and 78-nt RNAs when covered by two and three ribosomes respectively. Xrn1 arrests occur 17nts upstream of ribosomal A-site first residues (Pelechano *et al*., 2015). Using probe prG in primer extension experiments, 48- and 78-nt cDNA products are expected.

Supplementary Fig. 5

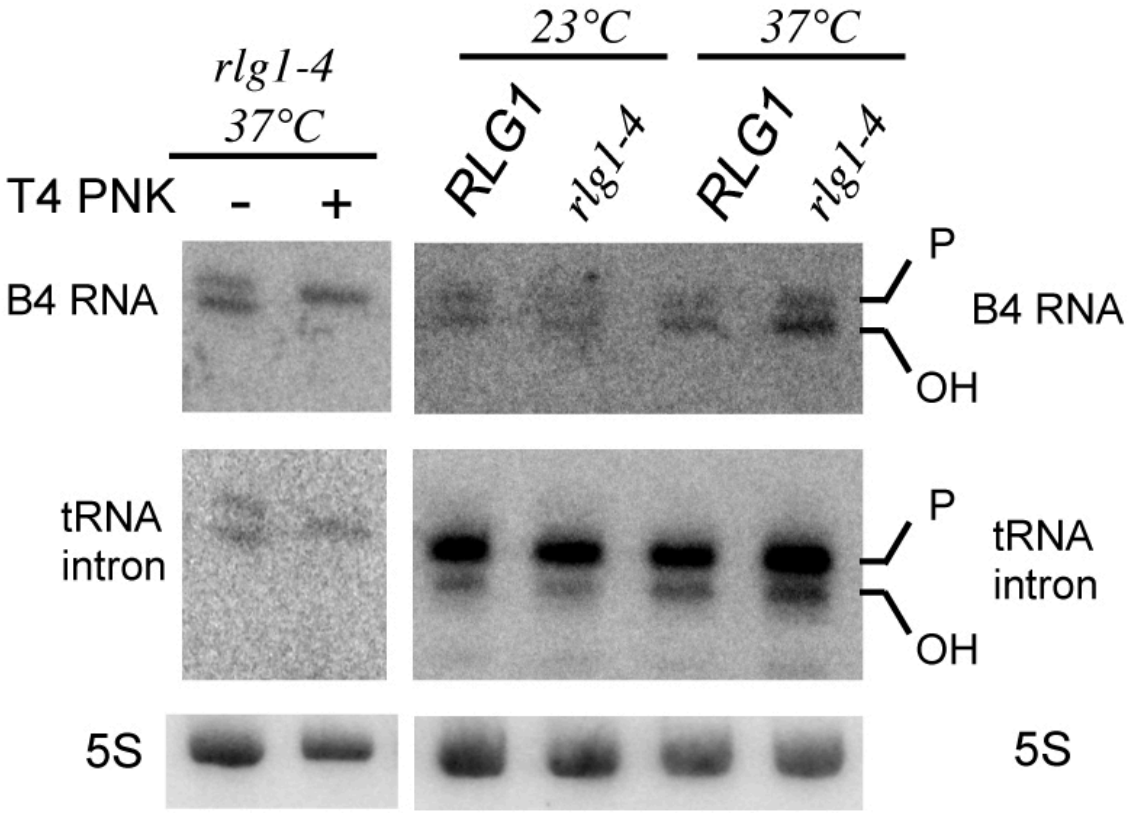

Supplementary Fig. 5: Endonucleolytically cleaved 5'-OH RNAs are phosphorylated by Rlg1/Trl1, related to Fig. 5. 5'-OH and 5'-P extremities of B4 RNAs and introns of $tRNA^{leu}$(CAA) as control RNAs of Rlg1 inactivation were analysed according to a method previously described [20]. 12% PAGE followed by northern blot analysis using probe prA to detect B4 RNAs, and probe prM to detect introns of $tRNA^{leu}$(CAA) (Wu and Hopper, 2014). Treatment using Polynucleotide kinase (PNK) of total RNA from *rlg1-4* mutant strains grown at 37°C determines the 5'-OH and 5'-P positions of RNAs of interest. The 5S rRNA served as a loading control.

Supplementary Fig. 6

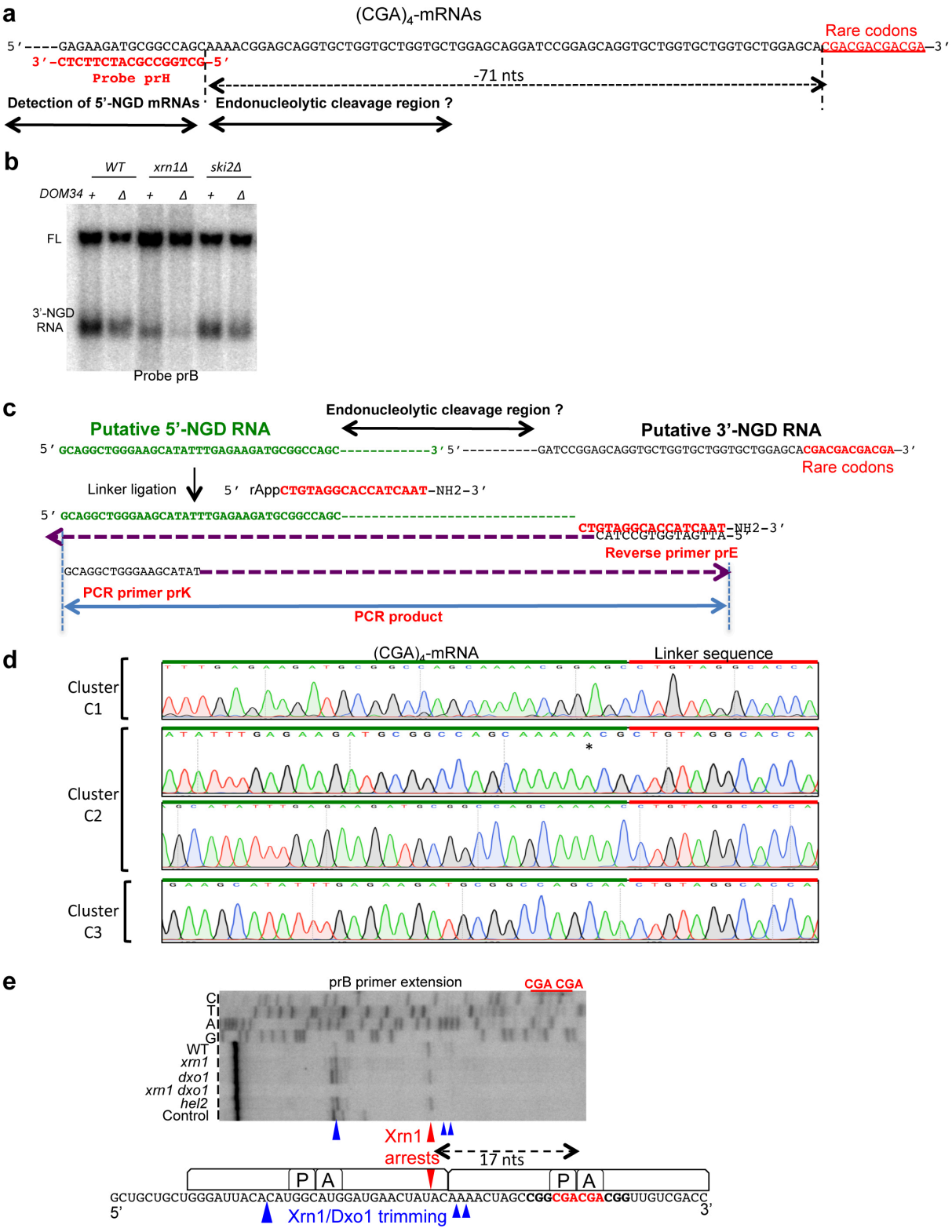

Supplementary Fig. 6: Analysis of $(CGA)_4$-mRNAs, related to Fig. 6. (**a**) Partial sequence of $(CGA)_4$-mRNA showing region upstream the four CGA rare codons. Positioning of probes prH is indicated. (**b**) 1.4% agarose gel followed by northern blotting analysis using probe prB showing steady state levels of RNAs in *dom34* and other indicated mutant strains. Full length $(CGA)_4$-mRNA is noted FL, and the 3'-NGD RNAs are indicated. (**c**) 3'-RNA ligase mediated RACE. The region of potential endonucleolytic cleavage, the 3'- and 5'-NGD

RNAs are indicated. The putative 3'-extremity is shown ligated to the universal miRNA linker. Sequence of reverse primer prG and PCR primer prK are indicated. **(d)** Chromatogram representing sequences obtained from 3'-RACE experiments performed on total RNA from *ski2* mutant cells and the three cleavage clusters C1, C2 and C3. The asterisk indicates one nucleotide A mismatch found in sequences. **(e)** Primer extension experiments using probe prB to determine the 5'-end of the mRNA containing two contiguous CGA rare codons as described previously (Tsuboi *et al*., 2014). A schematic view of the ribosome positioning on this mRNA is shown below and Xrn1-specific arrest is indicated by a red arrowhead. Arrests dependent on Xrn1/Dxo1 activities are also indicated by blue arrowheads.

METHODS

Yeast Media, plasmids, strains, and oligonucleotides. The media, plasmids, strains of *S. cerevisiae,* and oligonucleotides used in this study are described in supplemental information.

Northern blot analysis. RNA Extracts and northern blots were performed as described previously (Sinturel *et al*., 2012). Total RNA was resolved by 8% TBE-Urea polyacrylamide or 1.4%TBE-Agarose gels. Blots were exposed to PhosphorImager screens, scanned using a Typhoon FLA 9500 (Fuji), and quantified with ImageJ software.

***In vitro* RNA digestion.** RNA digestion of 20od$_{260nm}$ of cell extracts were performed by using 1 unit of Xrn1 (Biolabs) in NEB buffer 3 at 25°C during 30 min unless otherwise indicated. NEB Buffer 3 was replaced by Kinase NEB buffer in all kinase assays in the presence or absence of Xrn1 (Fig. 5a). For RNase I treatment of cell extracts, 2OD$_{260nm}$ of extracts (prepared without heparin) were incubated with 0.5, 1 and 2 microl of RNase I (Invitrogen, 100 units/ml) 30 min at 25°C. For total RNA treatment, 5microg of RNA were digested 30 min at 25°C. All RNase treatments were followed by RNA extraction and northern blot analysis as described above.

Polysome Analysis. Yeast cells were grown exponentially to 0.8 OD$_{600}$ at 28°C and were harvested by centrifugation. Cell extracts were prepared as described previously in lysat buffer 10mM Tris pH7.4, 100mM NaCl and 30 mM $MgCl_2$, and heparin was only omitted for RNase I treatment (Hu *et al*., 2009). The equivalent of 20 OD$_{260nm}$ units of cell extract (80µg of total RNA) was then layered onto linear 10% to 50% sucrose density gradients. Sucrose gradients (10%–50% sucrose in 10 mM Tris-HCl [pH 7.4], 70 mM ammonium acetate, 30 mM $MgCl_2$) were prepared in 12 × 89 mm polyallomer tubes (Beckman Coulter). Polysome profiles were generated by continuous absorbance measurement at 254 nm using the Isco fraction collector. Peaks corresponding to monosomes, disomes, etc were collected in fraction and processed for northern blotting as described above.

Primer Extension. Radiolabeled primers (primers prA and prE for mRNA1, and primer prJ for for $(CGA)_4$-mRNA) were used and reverse transcriptase (ThermoFisher) was used to synthesize a single-stranded DNA toward the 5'-end of the RNA. The size of the labeled

single-stranded DNA was determined relative to a sequencing ladder (ThermoFischer Sequenase sequencing kit) on 5% TBE-Urea polyacrylamide gel. Oligonucleotides were radio-labeled with [γ -32P]ATP with the T4 polynucleotide kinase (Biolabs).

3'-end RNA mapping. Mapping was performed according to the 3'-RNA ligase mediated RACE method described previously [33] with minor modifications: Total RNA preparations were first 3'-dephosphorylated using T4 PNK 1h at 37°C without ATP and pre-adenylated linker (Universal miRNA cloning linker, NEB) ligation was performed during 4h at 22°C in the presence of truncated ligase 2 (NEB) [32]. Reverse transcriptase reactions were performed using reverse primer prE complementary to the linker sequence. PCR primer prF specific to mRNA1, or primer prK specific to $(CGA)_4$-mRNA, were used with primer prE in PCR reactions (Supplementary Fig. 3a and 6c). PCR products were purified, cloned into zero Blunt TOPO PCR Cloning vector (Invitrogen), transformed and plasmids sequenced.

SUPPLEMENTARY INFORMATION

Yeast Media, related to experimental procedure. Strains were grown in YPD medium or in synthetic minimum media (SD) (Adams *et al*., 1997). Minimal media was completed for auxotrophy, leucine, histidine and/or uracil were omitted to keep selection for plasmids when necessary. 200 μ g/ml G418 Sulfate (Geniticin, American Bioanalytical), 100 μ g/ml Hygromycin B (Sigma-Aldrich) and 100 μ g/ml ClonNat (Werner Bioagents) were added in YPD media plates to select for KanMX4, hphMX4 and NatMX6 respectively. For lithium inhibition, cells were pre-grown in synthetic minimum media without methionine, cysteine and tryptophan and then transferred to the same media with 200 mM LiCl (for 1 hour).

Strains used in this study, related to experimental procedure. Mutant strains were generated by the one-step gene replacement using PCR fragment of the NatMX6 cassette amplified from plasmid pFA6a-natMX6 (Hentges *et al*., 2005), with hphMX4 containing cassette amplified from pAG32 (Goldstein and McCusker, 1999) or by the KanMX6 cassette amplified by PCR from plasmid pFA6a-kanMX6 respectively. Correct integration was confirmed by PCR with primers. Cas9 mediated gene modification were performed by following the protocol developed by Haber's group (Anand et al., 2017) using plasmid bRA90 to insert *rlg1-4* mutation (Phizicky et al., 1992) in the yeast BY4241 genetic background (strain YLB304). See Supplementary Table 1 for strains, and Supplementary Table 2 for used primers.

Plasmids used in this study, related to experimental procedure. Yeast plasmids used in this study were constructed using standard molecular biology procedures. To construct pLB138 (mRNA1RZ) and plB127 ($(CGA)_4$-mRNA), p415ADH1 [41] was first digested by SpeI-XhoI. DNA fragments containing URA3 were amplified by PCR from pRS316 (Sikorski and Hieter, 1989) using primers olb592-olb593 and digested by Spe1-BamH1. In parallel, oligonucleotides olb-ins1-f and olb-ins1-r were annealed. All DNA fragments were ligated to build pADH1-URA3. pADH1-URA3 was then digested by BspEI-NdeI. Genomic DNA was amplified using primers olb594-olb596 and digested by BamH1-NdeI in order to insert an additional ORF (ORF2) in the 3'-region of *URA3*. In parallel, in order to insert a ribozyme sequence (Rz) just downstream URA3 sequence, oligonucleotides oLb625 and olb626 were

annealed and all DNA fragments were ligated to form pADH1-URA3-Rz-ORF2. To insert 4 CGA codons, oligonucleotides oLb640 and olb641 were annealed and all DNA fragments were ligated to form pADH1-URA3-$(CGA)_4$-ORF2. Additionally, oligonucleotides olb-2HA-f and olb-2HA-r were annealed and cloned into pADH1-URA3-Rz-ORF2 or pADH1-URA3-(CGA)4-ORF2 (XbaI-SpeI digestion). The resulting plasmids p415ADH1-2HA-URA3-Rz-ORF2 and p415ADH1-2HA-URA3-$(CGA)_4$-ORF2 were named p138 and p127 respectively. The resulting ORF sequence of the mRNA with 3'-Rz insertion is shown in Supplementary Fig. 1a. Plasmids $pDxo1_{WT}$ and $pDxo1_{mut}$ used for the expression *in vivo* of WT Dxo1-Flag or of a catalytic mutant of Dxo1 (E260A D262A) were both created using synthetized DNAs (Genecust) cloned in SalI- XbaI sites of pRS313 (synthetized DNA sequences in Table S4). Thermocompetent NEB10 Beta *E.coli* (Biolabs) were used for cloning; all the plasmids were verified by sequencing (Eurofins Genomics).

Supplementary Tables

Supplementary Table 1. Strains used in this study

Supplementary Table 2. Oligonucleotides used in this study

Supplementary Table 3. Synthetized DNA DXO1 sequences for plasmid constructions

Supplementary Table 4. Plasmids used in this study

Supplementary Table 1

Name	alias	genotype	ref.	
BY4741	WT	*MATa his3Δ1 leu2Δ0 met15Δ0 ura3Δ0*	euroscarf	
Y05329	*dom34*	*MATa his3Δ1 leu2Δ0 met15Δ0 ura3Δ0 dom34::kanMX4*	euroscarf	
BY11756	*met22*	*MATa his3Δ1 leu2Δ0 lys2Δ0 ura3Δ0 met22::kanMX4*	euroscarf	
Y04540	*xrn1*	*MATa his3Δ1 leu2Δ0 met15Δ0 ura3Δ0 xrn1::kanMX4*	euroscarf	
Y05307	*ski2*	*MATa his3Δ1 leu2Δ0 met15Δ0 ura3Δ0 ski2::kanMX4*	euroscarf	
YLB152	*dxo1*	*MATa his3Δ1 leu2Δ0 met15Δ0 ura3Δ0 dxo1::kanMX4*	euroscarf	
YLB177	*met22 xrn1*	*MATa his3Δ1 leu2Δ0 lys2Δ0 ura3Δ0 met22::kanMX4 xrn1::hphMX4*	this study	derivated from BY11756
YLB082	*ski2 dom34*	*MATα his3Δ1 leu2Δ0 lys2Δ0 ura3Δ0 ski2::kanMX4 dom34::natMX6*	this study	derivated from Y05307
YLB083	*xrn1 dom34*	*MATα his3Δ1 leu2Δ0 lys2Δ0 ura3Δ0 xrn1::kanMX4 dom34::natMX6*	this study	derivated from Y04540
YLB084	*met22 dom34*	*MATα his3Δ1 leu2Δ0 lys2Δ0 ura3Δ0 met22::kanMX4 dom34::natMX6*	this study	derivated from BY11756
YLB178	*dxo1 dom34*	*MATa his3Δ1 leu2Δ0 met15Δ0 ura3Δ0 dxo1::kanMX4 dom34::natMX6*	this study	derivated from YLB152
YLB179	*xrn1 dxo1 dom34*	*MATa his3Δ1 leu2Δ0 met15Δ0 ura3Δ0 dxo1::kanMX4 xrn1::hphMX4 dom34::natMX6*	this study	derivated from YLB178
YLB176	*xrn1 met22 dom34*	*MATα his3Δ1 leu2Δ0 lys2Δ0 ura3Δ0 met22::kanMX4 dom34::natMX6 xrn1::hphMX4*	this study	derivated from YLB177
YLB165	*dom34 RLG1+*	*MATa ade2-1 ura3 RLG1 dom34::natMX6*	this study	
YLB166	*xrn1 dom34 RLG1+*	*MATa ade2-1 ura3 RLG1 xrn1 dom34::natMX6*	this study	
YLB226	*rlg1-4 dom34*	*MATa ade2-1 ura3 rlg1-4 dom34::natMX6*	this study	derivated from *rlg1-4* strain from Eric Phizicky
YLB227	*rlg1-4 xrn1 dom34*	*MATa ade2-1 ura3 rlg1-4 dom34::natMX6*	this study	derivated from *rlg1-4 xrn1* strain from Anita Hopper
YLB302	*ltn1 dom34*	*MATa his3Δ1 leu2Δ0 met15Δ0 ura3Δ0 ltn1::kanMX4 dom34::natMX6*	this study	derivated from Y04540
YLB303	*hel2 dom34*	*MATa his3Δ1 leu2Δ0 met15Δ0 ura3Δ0 hel2::kanMX4 dom34::natMX6*	this study	derivated from Y04540
YLB304	*rlg1-4 xrn1 dxo1 dom34*	*MATa his3Δ1 leu2Δ0 met15Δ0 ura3Δ0 dxo1::kanMX4 xrn1::hphMX4 dom34::natMX6 rlg1-4*	this study	CAS9 gene modification Derivated from YLB179

Supplementary Table 2

Name	alias	Oligo used for	Sequence 5' to 3'
olb495		DOM34 deletion by natMX6	CATTCGTTGCTGCATCGTTGTCATTTTGTTCAATTATCGCATTCCTATCATAGCAAAAATCGGATCCCCGGGTTAATTAA
olb496		DOM34 deletion by natMX6	CGATTTATTATAGGGTTGCAAATTTTATGTGTACATTACTTTTTTCTTACATAGTAAATCGAATTCGAGCTCGTTTAAAC
olb497		DOM34 deletion verification	GCGTCATCTTCTAACACCG
olb498		DOM34 deletion verification	GTGAACAGGTTCAGACAACTTCAAAGC
olb372		XRN1 deletion by hphMX4	GTTTATTTTCTAAAGGATACTGTCTTCTTCCGTACTTATAATCGGGTTCACGATCTGTTTAGCTTGCCTTG
olb373		XRN1 deletion by hphMX4	CAATCCCCATTTGTTATAAGCTTTTTCTTAACAAGATCAACGATTAAATACCTCGTTTTCGACACTGGATG
olb379		XRN1 deletion verification	CTATTCTCACGATTAATGGTC
olb380		XRN1 deletion verification	ATGGGAGACGTGCAAAAGC
olb561		SKI2 deletion verification	GGAACGGATAGAGGTTTGAAAAAGG
olb562		SKI2 deletion verification	GCTTTGGTTCATCGGTGCTC
olb978		DXO1 deletion verification	CCGCAATTTTCGCAGCATG
olb979		DXO1 deletion verification	GGTTTACGCATTGCTTTTCATAG
olb592		Construction of pLB138 (URA3 insert /URA3_SpeI)	GACATACTAGTATGTCGAAAGCTACATATAAGGAACG
olb593		Construction of pLB138 (URA3 insert/URA3_BamHI)	GACATGGATCCTGCTCCAGCACCAGCACCAGCACCTGCTCCGTTTTGCTGGCCGCATC
olb Ins1-f		insert in 3' of URA3 BglII-NdeI sites	GATCCCCAGTAGATCTTCGTGGGTGACATATGCCCGGGCTCGAGTGATAAG
olb Ins1-r		insert in 3' of URA3 BglII-NdeI sites	TCGACTTATCACTCGAGCCCGGGCATATGTCACCCACGAAGATCTACTGGG
olb594		Construction of pLB138 (downstream ORF of URA3_BamH1I)	GACATGGATCCGGAGCAGGTGCTGGTGCTGGTGCTGGAGCAATGCAGATCTTCGTCAAGACG
olb596		Construction of pLB138 (downstream ORF of URA_Nde1I)	GATACCATATGTCAACCACCTCTTAGTCTTAAGAC
olb625		Construction of pLB138 (RZ insertion)	CCGGATCCACCGTCACGCGTTGTGTTTACGCGTCTGATGAGTCCGTGAGGACGAAACGGTG
olb626		Construction of pLB138 (RZ insertion)	GATCCACCGTTTCGTCCTCACGGACTCATCAGACGCGTAAACACAACGCGTGACGGTGGAT
olb640		Construction of pLB127 (CGA4 insertion)	CCGGAGCAGGTGCTGGTGCTGGTGCTGGAGCACGACGACGACGAATGCA
olb641		Construction of pLB1278 (CGA4 insertion)	GATCTGCATTCGTCGTCGTCGTGCTCCAGCACCAGCACCAGCACCTGCT
olb 2HA-f		insert 2HA in XbaI-SpeI	CTAGAGGATCTATGTACCCATACGACGTCCCAGACTACGCTTACCCATACGATGTTCCAGATTACGCCGGATCCA
olb-2HA-r		insert 2HA in XbaI-SpeI	CTAGTGGATCCGGCGTAATCTGGAACATCGTATGGGTAAGCGTAGTCTGGGACGTCGTATGGGTACATAGATCCT
olb138-rev		Construction of pLB138	CTTCCCAGCCTGCTTTTC
olb138-22f		Construction of pLB138-22 (with olb138-rev)	GCTGGGAAGAAGCAUAUUUGAGAAGAUGGGCCAGCAAAACGGAGC
olb138-23f		Construction of pLB138-23 (with olb138-rev)	GCTGGGAAGAAAGCAUAUUCUAGAAGAUGGCCAGCAAAACGGAGC
olb138-24f		Construction of pLB138-24 (with olb138-rev)	GCTGGGAAGAGCAUAUAGAUUUUUUUGCGGCCAGCAAAACGGAGC
olb917	prA	probe of mRNA1	ACGGTGGATCCGGATCCTGCTC
olb622	prB	probe of mRNA1	CCGGGCATATGTCAACCACCTC
olb621	prC	probe of mRNA1	GGCGTAATCTGGAACATCGTATG
olb994	prD	probe of mRNA1	CGTTTTGCTGGCCGCATCTTCTC
olb937	prE	complementary sequence to universal miRNA cloning linker	ATTGATGGTGCCTACAG
olb1101	prF	probe of mRNA1 , PCR pirmer for 3' RNA ligae mediated RACE	GCTAAGGTAGAGGGTGAAC
olb1058	prG	probe of mRNA1 mRNA	AATATGCTTCCCAGCCTG
olb1117	prH	probe of mRNA-CGA4	GCTGGCCGCATCTTCTC
olb933	prJ	for primer extension on mRNA-CGA4	GTTGTCGATGGTATCGGAAGATTC
olb1104	prK	probe of RNA-CGA4 , PCR pirmer for 3' RNA ligae mediated RACE	GCAGGCTGGGAAGCATAT
olb1075	prL	probe of RNA 11, RNA 41 and RNA 48	CTGGGAGGACTCGTC
olbCrisp1		Forward Template Cas9 mediated gene modification	AAGTGATTTTGCTAGAATGCTATATACCCATAATGTCATCGCTGTCGCAGAATATTGCGATGATTCATTTGAAGAACACA
olbCrisp2		Reverse template Cas9 mediated gene modification	TGTGTTCTTCAAATGAATCATCGCAATATTCTGCGACAGCGATGACATTATGGGTATATAGCATTCTAGCAAAATCACTT
olbCrisp3		Forward Cas9 mediated gene modification	TACCCATAATGTCACCGCTGGTTTT
olbCrisp4		Reverse Cas9 mediated gene modification	CAGCGGTGACATTATGGGTAGATCA
Olb1161	prM	probe of $tRNA^{leu}$(CAA)	(Wu and Hopper, 2014)
RNA 48		Oligoribonucleotide RNA ladder	GGAGCAGGUGCUGGUGCCUGGUGGUGAUCGCAGGACGAGUCCUCCCAG
RNA 15		Oligoribonucleotide RNA ladder	GACGAGUCCUCCCAG

Supplementary Table 2 (continued)

Name	alias	Oligo used for	Sequence 5' to 3'
olb378	scR1	detection of scR1 mRNA	GTCTAGCCGCGAGGAAGG
olb25S	25S	detection of 25S rRNA	ATCCGCTAAGGAGTGTGTAACAACTCACC
olb18S	18S	detection of 18S rRNA	AGCCATTCGCAGTTTCACTG
olb959	5S	detection of 5S rRNA	CTACTCGGTCAGGCTCTTAC
olb1112	5.8S	detection of 5.8S rRNA	CCAAGAGATCCGTTGTTGAAAG

Supplementary Table 3

Sequences
Synthetized DNA sequences
Sc WT Dxo1 used forconstruction of pDxo1wt
GTCGACGAGACACTAAGCTGCTTTTTGATCTGTGCTGAGCTGAGTGTCCTACCATATGATCACTCTTGTATCGTCTACTT ATAGAGGTTGTTAGTACCAACCTGCAAATACAATTGTTGGACCATACTACCACAAAAGGTTCTTTTCGTTGGTGTATCCT CACAAATAATGATTATTCCACCAAAATCACCAAATTATTGTGTCAAACTAACTGGGATTACCCCACTATTGATTTTTCCA GTTTTTCCGCAATTTTCGCAGCATGTTTTACTTTTATAATGGCATTGTTGCATTACAGCGCCAGTTGTAGGTATCGATGA TTTTATGTCAAAGTTTTCTTTCTAGCCAAACTCAGTTATGTCAACTGAACAAGATGCTGTTCTTGGATTGGCCAAAGATT TAGAAGGTATAAATTTGCTTACTGTGCCCAATCTCGAGAGAGGACACCAAAGTAAATTATGCAAAGAGAAAACTACTTCT GATTCATCTTCGTCAAGGAAGCCTTCACAACAGAGAGACAATTATAGAAAGAGACGTCCGAAACTTATATGTATCCCATA TACGTCTTTTCTGCATACTGGTATGCACAATTTTTTGACGAAACCACCAAGAGATATATTTCATGAAAGTAAAGAAGTAG CTCTGTTTACCAATGGCCGGGCTTATACAATCCTACGCAAAGACCTTATACCAAATTTGAAAGAAAGTATTGCTGAATTG TATGAAAGCTCGCTTCTTGAGGCAAAAAAGCGGAAAGTCCCGTATTTAGGCCATGACTTATTTGCTAATATTGATGAGTT CGTTCCCATGACAATATCCGAATTAGATAGTGTATCACCGTGTTTTTCATACATTGAGAACTGGATACTAGATAATCCTG GTAAGGATTTTAAGATCGGCAAGAAATTTACTGTTGTAACCACAAGACATCATATCGTAGATTTGACTATGCATCTCTTT AACAGGCGAAATAGACAAACGTCACTAATTGTAACTTATATGGGGGCGGGCCTTCTTTCATTTTGCAGAAATGTAAAAAA AGATTCTCAAATGTCCAAAGAGGGCATTTATTCAAATGATCCAAATATGAAGAAAATTTGCTATTCAGGATTTGAATTTG AAAATTGGGTAACCGAAAATTCCAAAGTCGCTGATTTAACTGGCTCTAAATGTCCTATTTTTTCTCTTGTAGAGAGTAAA CTTTCAGAAGAAATTGGTCTTTTAATTCGCTGCGAAATGGATGCATTCAATCCTGTTTCGGAGACAAACACAGAACTAAA GTGTTTTGCCCCATTATCAATGCACAATTCCAATCATAGGAGAAAACTTCTGAAAACGTGGGTACAGACGGGTTTATTAC CGAACTCAGATATCATGATAGGTTTGAGGGACAGTCATAGCGGTCAATTACTAGACATTCAATGGTACTCAAGGGACTTA TTATGTAAGAAATTCAATCACCCAGGTCTACCTACAAATAAAAAGGAACTTAACTATAATGCCCAAATTGCGGTAGAATG GTGTCATTATTGTATTGAAGCAATTTGTAAGCTGGTGGAGGCAAATATCTCTGACTATAGCAGTACAAAACCAGAATCAT TTGAAATCGGTATAGATACTAACAACGCCATCGTCATCACTAAACTTAAGACTACTCCAAGAAACGTAGAATTATTTGGA ATGggatccggtgctggtgctggtgctggagcagattataaagatgacgatgacaaggactacaaggacgatgatgacaa aggatccTAGTAAAGACGTGTATAATATATAATACTTTTCCGAGAAATATTTCATTTTCATTTTCGTAAAGTTGTTAACT ACGCTAAATATTAGTACTTTTCTTAAATTTATATGGGGAGCCCTTTTTTTCTATGAAAAGCAATGCGTAAACCAAATAAG CAGAATTTTGTAATAGATGAGCAACAATACTGAGAAGGTGATAACTATAAATTTATGTGGGTAGTACGATACCAGAATAC ATTGGAAGATGGCTCTATTAGCTTTATATCATGTTGTCTTCAGGCCTTCAAAACTTATAGTATAGGTAGATCATCTAGA
Sc Dxo1 mutant used for construction of pDxo1mut (E260A/D262A)
GTCGACGAGACACTAAGCTGCTTTTTGATCTGTGCTGAGCTGAGTGTCCTACCATATGATCACTCTTGTATCGTCTACTT ATAGAGGTTGTTAGTACCAACCTGCAAATACAATTGTTGGACCATACTACCACAAAAGGTTCTTTTCGTTGGTGTATCCT CACAAATAATGATTATTCCACCAAAATCACCAAATTATTGTGTCAAACTAACTGGGATTACCCCACTATTGATTTTTCCA GTTTTTCCGCAATTTTCGCAGCATGTTTTACTTTTATAATGGCATTGTTGCATTACAGCGCCAGTTGTAGGTATCGATGA TTTTATGTCAAAGTTTTCTTTCTAGCCAAACTCAGTTATGTCAACTGAACAAGATGCTGTTCTTGGATTGGCCAAAGATT TAGAAGGTATAAATTTGCTTACTGTGCCCAATCTCGAGAGAGGACACCAAAGTAAATTATGCAAAGAGAAAACTACTTCT GATTCATCTTCGTCAAGGAAGCCTTCACAACAGAGAGACAATTATAGAAAGAGACGTCCGAAACTTATATGTATCCCATA TACGTCTTTTCTGCATACTGGTATGCACAATTTTTTGACGAAACCACCAAGAGATATATTTCATGAAAGTAAAGAAGTAG CTCTGTTTACCAATGGCCGGGCTTATACAATCCTACGCAAAGACCTTATACCAAATTTGAAAGAAAGTATTGCTGAATTG TATGAAAGCTCGCTTCTTGAGGCAAAAAAGCGGAAAGTCCCGTATTTAGGCCATGACTTATTTGCTAATATTGATGAGTT CGTTCCCATGACAATATCCGAATTAGATAGTGTATCACCGTGTTTTTCATACATTGAGAACTGGATACTAGATAATCCTG GTAAGGATTTTAAGATCGGCAAGAAATTTACTGTTGTAACCACAAGACATCATATCGTAGATTTGACTATGCATCTCTTT AACAGGCGAAATAGACAAACGTCACTAATTGTAACTTATATGGGGGCGGGCCTTCTTTCATTTTGCAGAAATGTAAAAAA AGATTCTCAAATGTCCAAAGAGGGCATTTATTCAAATGATCCAAATATGAAGAAAATTTGCTATTCAGGATTTGAATTTG AAAATTGGGTAACCGAAAATTCCAAAGTCGCTGATTTAACTGGCTCTAAATGTCCTATTTTTTCTCTTGTAGAGAGTAAA CTTTCAGAAGAAATTGGTCTTTTAATTCGCTGCGCTATGGCTGCATTCAATCCTGTTTCGGAGACAAACACAGAACTAAA GTGTTTTGCCCCATTATCAATGCACAATTCCAATCATAGGAGAAAACTTCTGAAAACGTGGGTACAGACGGGTTTATTAC CGAACTCAGATATCATGATAGGTTTGAGGGACAGTCATAGCGGTCAATTACTAGACATTCAATGGTACTCAAGGGACTTA TTATGTAAGAAATTCAATCACCCAGGTCTACCTACAAATAAAAAGGAACTTAACTATAATGCCCAAATTGCGGTAGAATG GTGTCATTATTGTATTGAAGCAATTTGTAAGCTGGTGGAGGCAAATATCTCTGACTATAGCAGTACAAAACCAGAATCAT TTGAAATCGGTATAGATACTAACAACGCCATCGTCATCACTAAACTTAAGACTACTCCAAGAAACGTAGAATTATTTGGA ATGggatccggtgctggtgctggtgctggagcagattataaagatgacgatgacaaggactacaaggacgatgatgacaa aggatccTAGTAAAGACGTGTATAATATATAATACTTTTCCGAGAAATATTTCATTTTCATTTTCGTAAAGTTGTTAACT ACGCTAAATATTAGTACTTTTCTTAAATTTATATGGGGAGCCCTTTTTTTCTATGAAAAGCAATGCGTAAACCAAATAAG CAGAATTTTGTAATAGATGAGCAACAATACTGAGAAGGTGATAACTATAAATTTATGTGGGTAGTACGATACCAGAATAC ATTGGAAGATGGCTCTATTAGCTTTATATCATGTTGTCTTCAGGCCTTCAAAACTTATAGTATAGGTAGATCATCTAGA

Supplementary Table 4

Plasmid	Description	Marker	Reference
p138	expression of RNA1Rz	LEU2	This study
p127	expression of (CGA)4-mRNA	LEU2	This study
p127T	expression of (CGA)2-mRNA	LEU2	This study
pDxo1WT	expression of Dxo1 of S. cerevisiae from pRS313 plasmid derivative	HIS3	This study
pDxo1mut	expression of a catalytic mutant of Dxo1 of S. cerevisiae from pRS313 plasmid derivative	HIS3	This study
pFA6a-natMX6	natMX6 confers resistance to nourseothricin		{Hentges et al., 2005}
pAG32	hphMX4 confers resistance to hygromycin B		{Goldstein et al., 1999}
pRS316	Centromeric	URA3	(Sikorski et al., 1989
pRS313	Centromeric	HIS3	(Sikorski et al., 1989
bRA90	Cas9 mediated gene modification	LEU2	(Anand et al., 2017)

SUPPLEMENTARY REFERENCES

Adams, A., Gottschling, D.E., Kaiser, C.A., and Stearns, T. (1997). Methods in yeast genetics. Cold Spring Harbor Laboratory Press, Cold Spring Harbor, NY.

Anand, R., Beach, A., Li, K. and Haber, J. (2017) Rad51-mediated double-strand break repair and mismatch correction of divergent substrates. Nature 544(7650): 377–380

Gari, E., Piedrafita, L., Aldea, M., and Herrero, E. (1997). A set of vectors with a tetracycline-regulatable promoter system for modulated gene expression in Saccharomyces cerevisiae. Yeast *13*, 837-848.

Goldstein, A.L., and McCusker, J.H. (1999). Three new dominant drug resistance cassettes for gene disruption in Saccharomyces cerevisiae. Yeast *15*, 1541-1553.

Hatfield, L., Beelman, C.A., Stevens, A., and Parker, R. (1996). Mutations in trans-acting factors affecting mRNA decapping in Saccharomyces cerevisiae. Mol Cell Biol *16*, 5830-5838.

Hentges, P., Van Driessche, B., Tafforeau, L., Vandenhaute, J., and Carr, A.M. (2005). Three novel antibiotic marker cassettes for gene disruption and marker switching in Schizosaccharomyces pombe. Yeast *22*, 1013-1019.

Janke, C., Magiera, M.M., Rathfelder, N., Taxis, C., Reber, S., Maekawa, H., Moreno-Borchart, A., Doenges, G., Schwob, E., Schiebel, E., *et al*. (2004). A versatile toolbox for PCR-based tagging of yeast genes: new fluorescent proteins, more markers and promoter substitution cassettes. Yeast *21*, 947-962.

Pelechano, V., Wei, W., and Steinmetz, L.M. (2015). Widespread Co-translational RNA Decay Reveals Ribosome Dynamics. Cell *161*, 1400-1412.

Sikorski, R.S., and Hieter, P. (1989). A system of shuttle vectors and yeast host strains designed for efficient manipulation of DNA in Saccharomyces cerevisiae. Genetics *122*, 19-27.

Wu, J. & Hopper, A. K. Healing for destruction: tRNA intron degradation in yeast is a two-step cytoplasmic process catalyzed by tRNA ligase Rlg1 and 5'-to-3' exonuclease Xrn1. Genes Dev 28, 1556-1561 (2014).